REPORT DOCUMENTATION PAGE

AFRL-SR-AR-TR-05-

0357

1. REPORT DATE (DD-MM-YYYY)	2. REPORT TYPE	3. DATES COVERED (From - To)
10/08/2005	Final Performance Report	01/May/03 - 28/Feb/05

4. TITLE AND SUBTITLE

Magnetically Responsive Optical Nanoprobes (MagRONs) and Systems

5a. CONTRACT NUMBER

5b. GRANT NUMBER
F49620-03-1-0297

5c. PROGRAM ELEMENT NUMBER

6. AUTHOR(S)

Prof. Roul Kopelman

5d. PROJECT NUMBER

5e. TASK NUMBER

5f. WORK UNIT NUMBER

7. PERFORMING ORGANIZATION NAME(S) AND ADDRESS(ES)

The regents of the University of Michigan,
Division of Research Development and Administration,
1058 Wolverine Tower DRDA,
Ann Arbor, MI 48109-1274

8. PERFORMING ORGANIZATION REPORT NUMBER

Final performance report
(3rd report).

9. SPONSORING / MONITORING AGENCY NAME(S) AND ADDRESS(ES)

USAF, AFRL
AF OFFICE OF SCIENTIFIC RESEARCH
4015 WILSON BLVD ROOM 713
ARLINGTON VA 22203-1954
CAROL A. MONOHAN 703-696-5993 carol.monohan@afosr.af.mil

NL

10. SPONSOR/MONITOR'S ACRONYM(S)
AA

11. SPONSOR/MONITOR'S REPORT NUMBER(S)

12. DISTRIBUTION / AVAILABILITY STATEMENT

Approve for Public Release: Distribution Unlimited

13. SUPPLEMENTARY NOTES

14. ABSTRACT

Magnetically Modulated Optical Nanoprobes (MagMOONs) are chemical and physical probes that blink in response to rotating magnetic fields. The blinking distinguishes probe fluorescence from autofluorescent backgrounds, allowing chemical measurements based on fluorescence spectrum, even in the presence of background. In addition, the blinking rate reveals information about particle size and local viscosity on a single probe level. We expanded our capabilities for fabrication of MagMOONs, while developing new applications and techniques for the MagMOON platform. We made MagMOONs that sense pH, developed a general method to make uniformly magnetic half-shell MagMOONs by depositing magnetic materials onto a wide range of nanospheres, and improved our immunoassay techniques. Brownian MOONs (300 nm) were used to observe biomechanical rotation inside living macrophages. These tools have promising applications for disease and pathogen detection, measuring material properties and mechanical forces on the nanoscale, and observing cell response to drug candidates and other stimuli.

15. SUBJECT TERMS

16. SECURITY CLASSIFICATION OF: Non Classified			17. LIMITATION OF ABSTRACT	18. NUMBER OF PAGES	19a. NAME OF RESPONSIBLE PERSON
a. REPORT Non Classified	b. ABSTRACT Non Classified	c. THIS PAGE Non Classified		70	Prof. Raoul Kopelman
					19b. TELEPHONE NUMBER (include area code) (734) 764-7541

BAA 01-42, ADDENDUM 3, SPECIAL FOCUS AREA: BIO-MAGNETIC INTERFACING CONCEPTS (BioMagnetICs).

Award number F4960-03-1-0297

Final Performance Report

Title: Magnetically Responsive Optical Nanoprobes (MagRONs) and Systems

Project Dates: 1 May 2003 – 28 Feb 2004.

Raoul Kopelman, Ph.D. Principal Investigator

Kasimir Fajans Collegiate Professor of Chemistry, Physics and Applied Physics

The University of Michigan

Martin A. Philbert, Ph.D. Co-Principal Investigator

Associate Professor of Toxicology, Associate Dean of the School of Public Health,

The University of Michigan

Address:

Raoul Kopelman

University of Michigan Chemistry

930 N. University Ave.

Ann Arbor, MI 48109-1055

Email: kopelman@umich.edu

Phone: (734) 764-7541

Fax: (734) 936-2778

Note: *we updated the acronym for our microscopic sensors from MagRONs (Magnetically Responsive Optical Nanoprobes) to MagMOONs (Magnetically MOdulated Optical Nanoprobes) because the term "modulated" describes the technique more accurately, and because the metal-capped particles look like moons.*

Contents:

Executive Summary:

There are two principal approaches to nanotechnology, bottom-up and top-down. The top-down approach uses lithography, etching, and controlled deposition of materials to build nanodevices onto a macroscopic surface such as wafers, or occasionally wires and fiber tips. The bottom-up approach uses wet-chemistry to assemble monomers or crystals into large quantities of polymeric or inorganic nanoparticles for materials additives, immunoassay tags, or biomedical capsules. The MagMOONs project combined advantages from both approaches to produce roving devices with controlled multifunctional and synergistic magnetic, photonic, and chemical properties for mechanical and chemical sensing and effecting. The roving approach also does away with the need for electrical and mechanical nano-links that fasten the probes to macroscopic surfaces such as wires, or fiber tips. Rather, photons and magnetic fields remotely interrogate and control the nanodevices. In addition, the platform design makes it simple to control device size, chemistry, and magnetic and fluorescent properties creating tools that are able to explore scales unavailable to free dyes and molecules. At the same time, the optical detection methods offer greater sensitivity than purely magnetic read outs, and allow interfacing with standard microscopes and plate readers.

Depositing materials onto one hemisphere of a nanosphere breaks the spherical symmetry of the nanosphere, creating a device with optical, chemical, and electronic properties that depend on which side is facing. For instance, if the deposited material is opaque or reflective (e.g. metal), the nanosphere reflects and fluoresces different amounts of light in different orientations, allowing its orientation to be tracked in time (figure 1). When these "Modulated Optical Nanoprobes" rotate, their fluorescence intensity blinks, allowing their fluorescent properties to be distinguished and separated from autofluorescent backgrounds. This background separation allows sensitive local chemical analysis based on MOON spectrum, even in the presence of background. In addition, tracking rotation of these Modulated Optical Nanoprobes (MOONs) in time reveals any torques acting on the particle from magnetic fields, Brownian torques, rotational biomechanical transport in macrophages, and chemical attraction. The rotation also reveals fluid vorticity, translation/rotation coupling (rolling traction), and the opposing torque of the medium's viscous drag and elasticity.

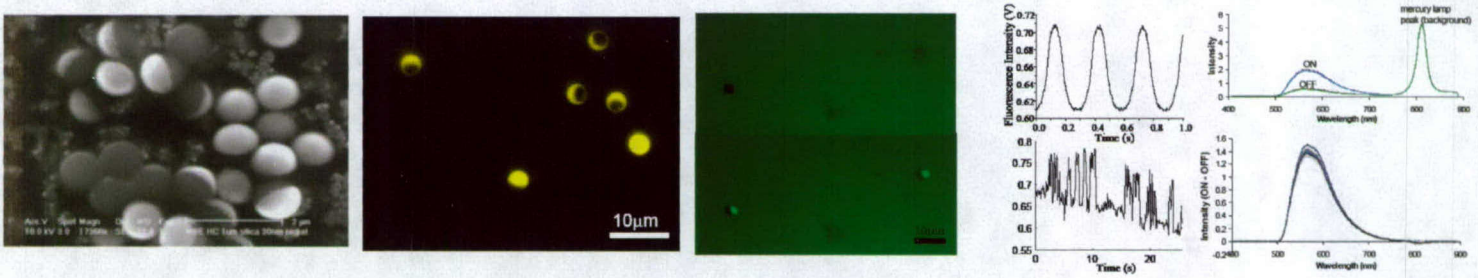

Figure 1. (a) A TEM image of 970 nm polystyrene nanospheres coated with cobalt half-shells using vapor deposition. (b) Fluorescent image of 3.4 μm MOONs each rotating individually due to Brownian torques. (c) Two 4.5 μm magnetically modulated MOONs (MagMOONs) rotating and blinking synchronously (top and bottom panels). (d) Intensity time series for 4.5 μm magnetically modulated MagMOONs (top) and 2 μm Brownian MOONs (bottom). (e) (top) "ON" and "OFF" spectra from chain-shaped MagMOONs; (bottom) ON minus OFF spectra subtracts off constant background such as mercury lamp background at 800 nm.

During the grant period, we expanded our capabilities for MagMOONs fabrication, while developing new applications and techniques for the MagMOON platform. We made MagMOONs that sense pH, developed a general method to deposit magnetic half-shells onto nanospheres to make MagMOONs with uniform magnetic properties from nanospheres with a wide range of sizes and compositions, and used 300 nm Brownian MOONs to observe biomechanical rotation of single MOONs inside living macrophages (figure 2). These tools have promising applications for disease detection and diagnosis, measuring material properties and mechanical forces on the nanoscale, and observing cell response to drug candidates and other stimuli.

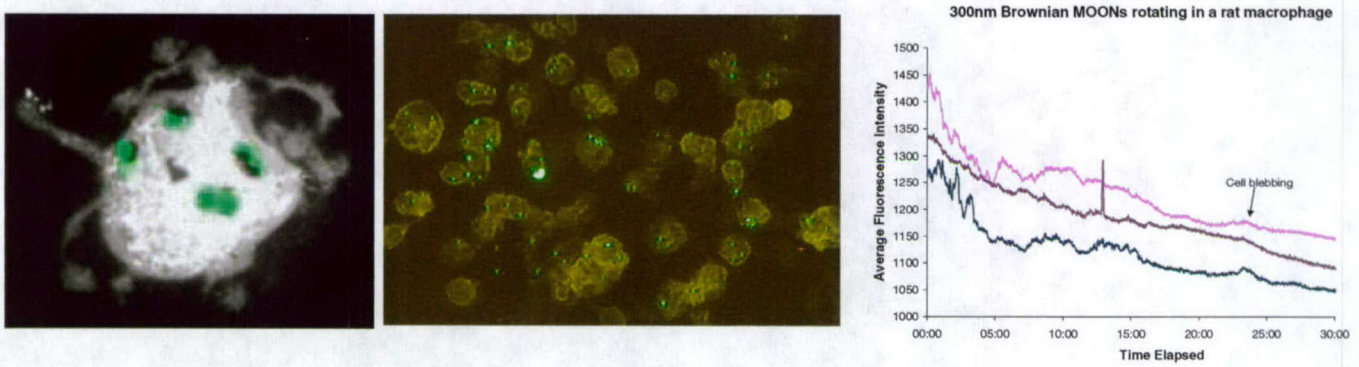

Figure 2. (a) A macrophage containing 4.5 μm MOONs. (b) Many macrophages containing 300 nm diffraction limited MOONs. (c) Intensity time series for individual 300 nm MOONs in a macrophage rotating due to biomechanical forces. The rotation ends after the cell dies; bleaching is also evident.

This grant has helped support 5 graduate students, 5 postdocs, and 2 professors. The grant has also led to the publication of ten articles, one thesis and one article in preparation.

Accomplishments/New Findings:

During the project we progressed on two parallel tracks, as shown in figure 3 below. We developed new nanoparticle architectures and fabrication techniques. At the same time, we developed new applications for the MagMOON platform.

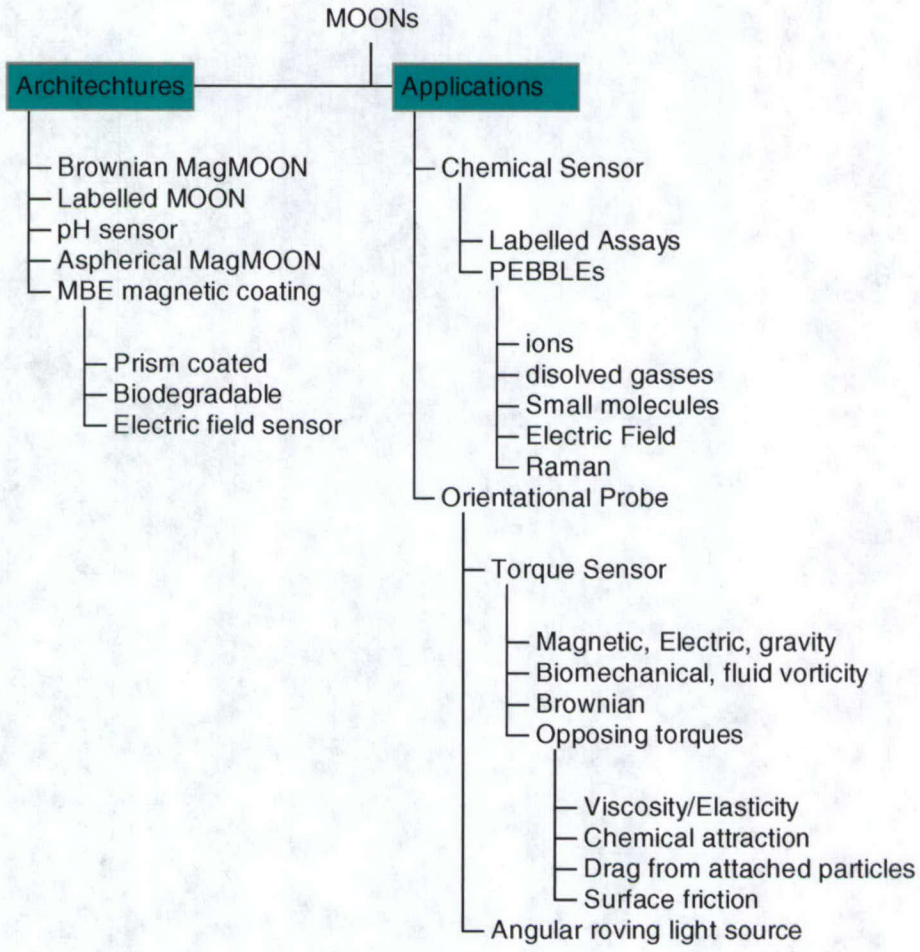

Figure 3: Expanding architectures and applications for the MagMOON platform.

I. Sensor Fabrication

During the term of the project, we enhanced our fabrication capabilities and produced new types of nanoparticles (Figure 4). Using molecular beam deposition (MBD), we can now make any particle into a MagMOON by depositing magnetic material onto the surface of the microsphere. Fine control over the thickness and composition creates highly uniform magnetic particles, and allows systematic optimization of magnetic, optical, chemical, and electronic properties. We have also discovered that we can produce arches in the metal

coating which may lead to enhanced optical properties. Enhanced fluorescence is observed for metal-capped particles due to reflection from the metal; for particles smaller than the diffraction limit, plasmon resonance and quantum effects become important. We fabricated prism shaped nanoparticles with controllable plasmon resonances, and are the first to attach them to silica nanoparticles. By attaching the prisms to the surface of MagMOONs, coupling between particles is enhanced leading to novel applications such as Surface Enhanced Raman Spectroscopy (SERS). All of these developments have applications for chemical sensing and materials research.

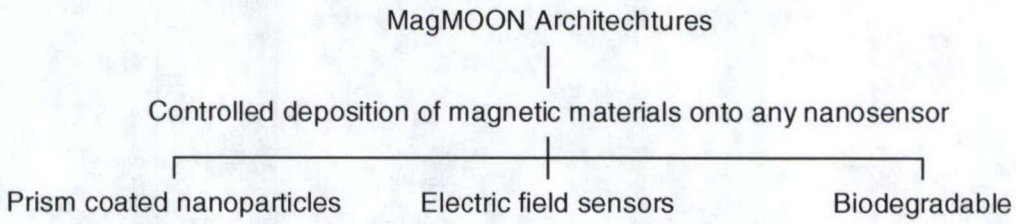

Figure 4: Novel MagMOON Architectures.

a) Materials and Methods

Polystyrene nanospheres were purchases from BangsLabs (Fishers, IN), ferromagnetic microspheres were purchased from Spherotech (Libertyville, IL). 300 nm silica nanospheres with pH dyes were produced in our lab. Molecular Beam Epitaxy (MBE) deposition was performed at Dr. Roy Clarke's laboratory (University of Michigan) with the help of Vladimir Stoica. All the scanning tunneling transmission electron microscopy (STEM) images were acquired on a Joel 2010F instrument with the help of Dr. Kai Sun in the EMAL facility at the University of Michigan. TEM images were acquired on the Philips CM12 electron microscope. SEM images of the MBE particles were taken using a Phillips XL30 Field Emission Gun Scanning Electron Microscope. MOONs were placed in glycerol-water solutions with different viscosities and put into a demountable 100 μm quartz sample chamber (Starna, Atascadero, CA, USA). The small thickness of this cell prevented convection from affecting the particle motion. The particles were viewed with an Olympus IMT-II (Lake Success, NY, USA) inverted fluorescence microscope. Fluorescence spectra were acquired using an Acton Research Corp. spectrograph and a Hamamatsu HC230 CCD interfaced with an Intel Pentium computer. Images and videos of Brownian MOONs were

acquired with a Photometrics Coolsnap ES CCD camera from Roper Scientific, or a Nikon Coolpix 995 camera.

b) MagMOON Miniaturization

Preparation of 300 nm pH sensing MagMOONs

Elucidating cellular and physiological responses to pathogens, toxins, drugs, and other stimuli is a major challenge of medicine and biology. MagMOONs promise to improve intracellular measurements where autofluorescence has severely limited the range of dyes and samples that can be detected with reasonable signal to noise ratios. Our recently developed Photonic Explorers for Bioanalysis with Biologically Localized Embedding (PEBBLE)[1-3] nanosensors measure concentrations of ions and small molecules within a single cell, rapidly, sensitively, with high spatial resolution, and without interference from cellular proteins. PEBBLEs can be introduced into cells using a standard delivery mechanism common to all sensor types regardless of the analytes they sense. Combining PEBBLEs with MagMOONs will increase the sensitivity to intracellular analytes using fewer probes. Magnetic modulation will increase the range of dyes that can be used, including blue and ultraviolet excited dyes as well as weakly fluorescing dyes. MagMOONs can also be used in a wider range of samples, including highly fluorescent cells, tissues, and stained cells.

Initial demonstrations of the MagMOON principle used larger particles, approximately 4 μm diameter microspheres or long chains of 1 μm particles. In order to introduce MagMOONs into cells with minimal perturbation, it is necessary to reduce their size to submicron dimensions. We have successfully produced pH sensitive 300 nm MagMOONs. The MagMOONs consist of a silica matrix embedded with: barium ferrite nanoparticles to provided magnetic orientation, and a ratiometric pH sensitve dye, dextran-linked SNARF (Molecular Probes, Eugene OR).

Barium ferrite (BaM) crystals of 30 and 60 nm diameter were a donation from Toda Kogyo Corp. The crystals were ground for one hour in an aluminum oxide mortar and pestle. Approximately 200 mg of ground BaM were sonicated for one hour in 24 mL of an ethanol solution that contained 2M ammonia and 6M deionized water. After sonication, the suspension was centrifuged for 15 minutes at 500 RPM to remove aggregates. 24 mL of supernatant were transferred to a 100 mL round bottom flask. To the same flask was added

800 µL dextran linked SNARF pH indicator dye (5 mg dye per 1 mL deionized water). The polymerization reaction was initiated by adding 70 µL tetraethylorthosilicate (TEOS). The reaction was allowed to progress for 2 hours, after which the silica nanoparticles were removed by vacuum filtration.

To prepare MagMOONs, a suspension of BaM/SNARF silica nanoparticles in deionized water was deposited on a glass microsope slide. After the water evaporated, the nanoparticles were coated with aluminum by vapor deposition. The MagMOONs were magnetized by placing the slide in a magnetic field. The MagMOONs were removed from the microscope slide by gently stroking the slide with an artist's paintbrush. Figure 5 shows SEMs, spectra, and modulation from the MagMOONs.

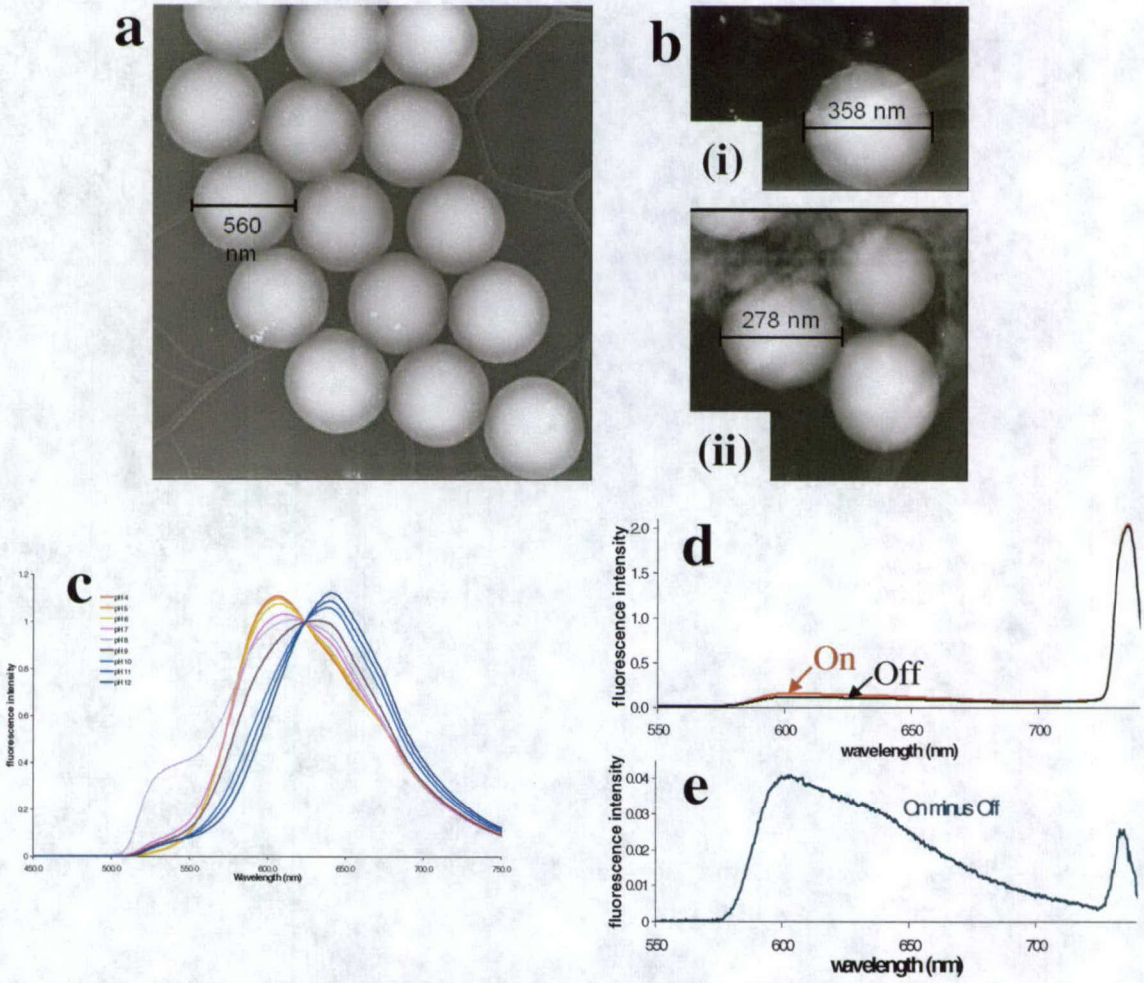

Figure 5. pH sensitive silica MagMOONs. (a) TEM image of 600 nm blank silica particles containing no magnetic materials or dye [a control]. (b) (i) and (ii) TEM images of 300 nm particles containing Barium ferrite and SNARF dye. Capping these particles with aluminum will make them into MagMOONs. (c) Fluorescence emission spectra from the particles taken at varying pH. The ratio of two emission peaks varies with pH. (d) Magnetic modulation of the 300nm metal-capped MagMOONs, "on" and "off" spectra. (e) Subtracting average "on" minus "off" reduces background signal 100 fold, separating the MagMOON signal from background.

c) Fabrication of uniform half-shell magnetic microspheres/MagMOONs using Molecular Beam Deposition (MBD)

There are two principle approaches to fabrication of nanodevices: top-down, and bottom-up. The top-down approach builds nanodevices by lithography, eteching and controlled deposition of materials onto a flat substrate (such as a wafer). The bottom-up approach builds nanodevices by assembling monomers, dyes, and crystals into nanoparticles using wet-chemistry. Both approaches have advantages: the top-down approach allows fine and systematic control of the material and direct electrical interfacing; while the bottom-up approach allows rapid production, flexibility of design, and creation of untethered devices for *in situ* control and measurement. Combining bottom-up synthesis of nanosphere sensors with top-down methods for controlled deposition of magnetic and semiconductor materials produce hybrid particles with well controlled magnetic, optical, electronic, and chemical properties for *in situ* use.

Potential applications of coating magnetic materials onto nano- and microparticles using MBD include: 1) Making any current nanosphere sensor into a MagMOON by coating with magnetic material. 2) Fabricating controlled (~1 Å thickness resolution) uniform magnetic particles for use in MRI, cell separation, magnetic based assays, and other applications of magnetic microspheres. The use of uniform, particles is especially important in applications that work on single particle levels. 3) Different batches of MagMOONs coated with varying amounts of magnetic material will have a different maximum rotation rate, and each batch can be differentiated based on rotation rate. This signal differentiation enables simultaneous measurements from different populations of MagMOONs that sense different analytes. 4) Controlling the materials deposited opens up new magnetic, optical, and chemical properties for nanosphere sensors. In addition, the geometry of the spherical particles may create new electronic and magnetic properties for magnetic storage and read out. 5) Geometries such as the first reported metallic arches may create new optical properties.

MagMOONs were produced by coating a uniform half-shell of ferromagnetic cobalt or iron onto nanospheres and microspheres using ultra high vacuum (UHV) vapor deposition in Professor Roy Clarke's lab (University of Michigan). Uniformly sized polystyrene spheres

50 nm, 300 nm, 970 nm 2 μm, and 3.4 μm in diameter (purchased from Bangs Labs and Polysicences Inc.) were coated with cobalt or iron. The metal was deposited at a rate of 1-4 Å/s, providing fine control of the layer thickness.

The cobalt coating was characterized during deposition using a RHEED (Reflection High-Energy Electron Diffraction) instrument (k-space, Inc.). Figure 6 shows the RHEED image for 200 nm of cobalt grown on diffuse microspheres and on the microscope slide. These rings indicate that the deposited cobalt is polycrystalline. As the coating thickness increased these rings became sharper and more intense. Control over the deposition rate thickness and materials will lead to novel properties.

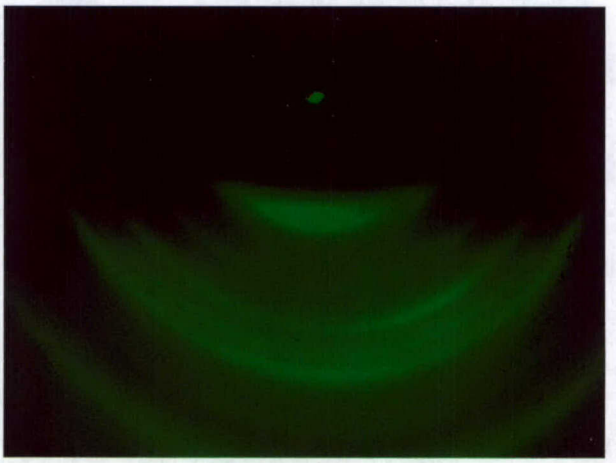

Figure 6. RHEED image indicating polycrystalline deposition of cobalt on the nanospheres.

The half-shell particles produced are smoothly coated with controllable unparalleled uniformity in amounts of magnetic material. The process works for a wide range of particle sizes, shapes, and compositions, as well as for different material matrixes, providing a universal method of producing MagMOONs. Control over amount of deposited material solves the longstanding problem of creating magnetic micro and nanoparticles with uniform magnetic properties. Magnetic uniformity is especially important for single particle force and torque studies. Indeed, a recent study of particles from 5 commercial companies demonstrated that the particles had variations in magnetic responsiveness varying between 30-80% from the average value (U.O. Häfeli, R. Ciocan, and J.P. Dailey, European Cells and Materials **3**, 34 (2002).

The use of top down deposition of magnetic materials solves the longstanding problem of non-uniformity in commercially made magnetic particles (usually produced using

purely bottom up chemical synthesis). The simple control over material composition, also increases the effective magnetic moment of the particles compared to iron oxide, and allows control over coercivity, and addition of protective layers of materials including metals and silica. After the spheres were coated, SEM images were taken, Figure **7**. The top row of Figure **7** depicts magnetic half-shell particles fabricated using UHV vapor deposition, where the direction of the arrow indicates increasing size, from 300 nm to 3.4 μm. For comparison, the bottom row of Figure 7 shows similarly sized commercially made magnetic particles. These commercially made particles appear to be rough, irregular in shape (>20% deviation from a perfect circle for 340 nm particles) and have a large variation in size, especially for smaller particles; by comparison, the cobalt coated particles are smooth, have close to spherical shape (<10% deviation from a perfect circle for 300 nm particles), and have a narrower size distribution. To investigate variations in coating uniformity from particle to particle, the 3.4 μm cobalt coated particles were imaged with bright field (transmission) microscopy. On a flat surface the 30 nm of cobalt attenuated light by 10.6%. The images, Figure **8**, revealed particles with almost identical transmission profiles and small variations in maximum transmission (6% standard deviation). Large deviations in the amount of magnetic material will affect magnetic responsiveness (U.O. Häfeli, R. Ciocan, and J.P. Dailey, European Cells and Materials **3**, 34 (2002). In our own experiments, using commercially available 4.4 μm magnetic microspheres for microrheology, we observed that measurements varied significantly from sphere to sphere. With uniform magnetic particles, more accurate experiments could be designed, so as to better probe microrheology and molecular interactions. Additionally, this fabrication technique could be used to modify solid state sensors into MagMOONs, by the simple step of depositing a ferromagnetic metal onto the surface of a sensor.

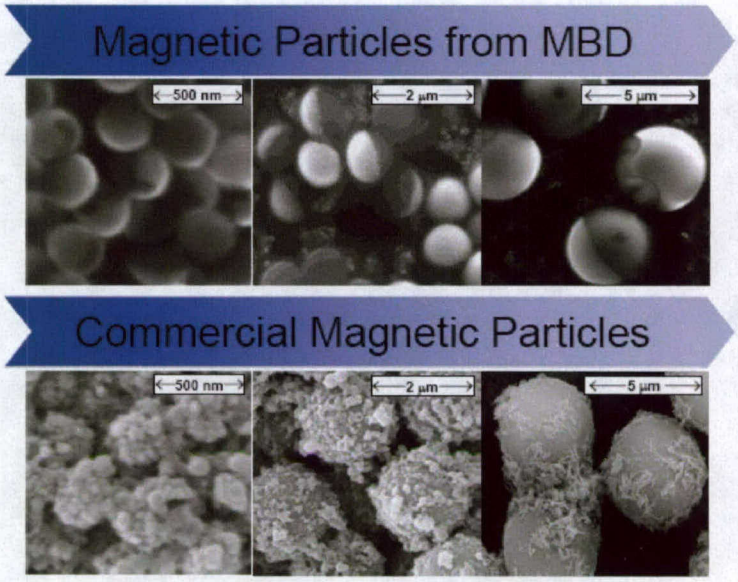

Figure 7. Scanning electron microscopy (SEM) images of various magnetic particles, where the arrow indicates increasing size. Top Row: Magnetic particles fabricated by coating polystyrene spheres that are 300 nm in diameter with a layer of 20 nm of cobalt; 1.0 μm in diameter spheres coated with 30 nm of cobalt; and 3.4 μm spheres coated with 20 nm of cobalt. Bottom Row: Commercially made magnetic particles that are 330 nm, 1.89 μm, and 4.4 μm in diameter (Spherotech, Inc.).

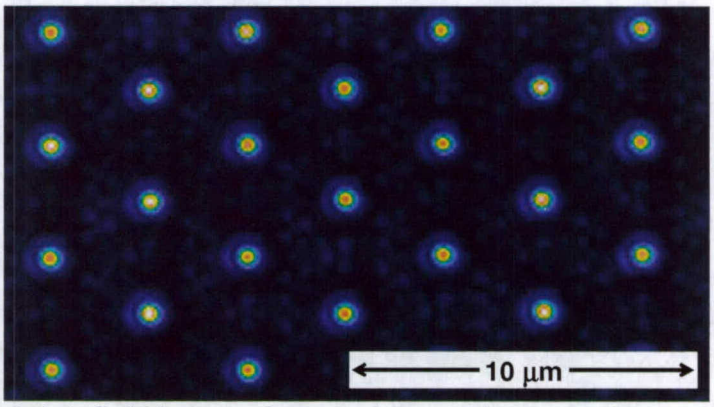

Figure 8. A brightfield image of a monolayer of 3.4 μm polystyrene microspheres, coated with 30 nm of cobalt, where the pseudocolor scales from blue, representing least transmission, to white, representing highest transmission.

Also evident from the SEM images are arch-like structures in the deposited metal of the 300 nm and the 3.4 μm cobalt-coated spheres, top row of Figure 7.These arches are formed by two methods, either allowing the substrate temperature to exceed the glass transition temperature of polystyrene (≈95°C), or by using an angled deposition so one particle shadows its neighbor from the cobalt atomic beam flux. If the substrate temperature was above the glass transition temperature of polystyrene, then the particles could fuse

together, and when broken apart leave an arch-like structure on the surface of the sphere. The eye-shaped patterns inside the arches provides evidence for melting and sticking together for the 3.4 μm spheres, top right of Figure 7. Alternatively, when coating occurs at a significant angle normal to the substrate, in our case ~40°, then the arches could form from shadowing effects, as observed on silica coated particles. The presence of these arches could affect the magnetic properties of the cobalt film. Additionally, the lightning rod effect creates large electromagnetic field enhancements at the tips with applications for SERS (surface enhanced Raman spectroscopy) and for non-linear optical effects, similar to enhancements seen with prism shaped particles *(J.C. Hulteen, R.P. Van Duyne, J. Vac. Sci. Technol. A* ***13****, 1553-1558 (1995)* and nanocrescents *Y. Lu, G. L. Liu, J. Kim, Y. X. Mejia, and L. P. Lee, Nano Lett.* ***5****, 119 (2005).*

To further characterize the magnetic half-shell particles fabricated by UHV vapor deposition, MOKE magnetometry in longitudinal geometry was performed on 50 nm spheres coated with a 20 nm of cobalt. The presence of these nanospheres enhanced the coercivity of the planar cobalt layer by more than a factor of three, compared to bulk values, Figure 9a. A similar effect for polar MOKE magnetometry, studied by Albrecht et al. (Nat. Mater. **4**, 203 (2005))., has also been observed in magnetic multilayers of cobalt and palladium grown on polystyrene nanospheres, which has applications in computer memory and magnetic storage. The magnetic hysteresis curves for the 50 nm spheres with the magnetic field applied parallel to the substrate, Figure 9, have a square-like shape, indicating that the easy axis of magnetization is parallel with the substrate surface as well as with the nanosphere surface.

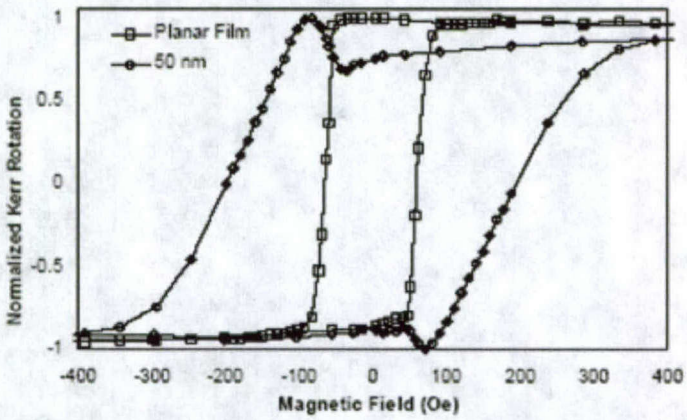

Figure 9. Characterization of uniform magnetic particles using a) magnetic hysteresis curves obtained by magneto optic Kerr effect (MOKE) magnetometry on 50 nm polystyrene spheres, coated with 20 nm of cobalt. The asymmetries and kinks near zero-field are due to the vectorial nature of MOKE which simultaneously probes the in plane and out of plane components of the magnetization. b) Time series of the fluorescence intensity from a 3.4 μm cobalt coated MagMOON rotated by a 0.25Hz magnetic driving field.

In addition to forming magnetic half-shell particles on a plane, we removed them from the glass substrate, suspended them into solution, and rotated them with an external magnetic field. Figure 10 shows the time series for a 3.4 μm fluorescent polystyrene microsphere with a cobalt layer of 20 nm, modulated in an external rotating magnetic field at a driving frequency of 0.25 Hz. Upon demodulation, by subtracting "On" minus "Off," the background can be removed, thus allowing for more sensitive fluorescence measurements. The same process could be utilized with almost any nanosphere or microsphere, thereby allowing nanosensors or microsensors to be modified into MagMOONs.

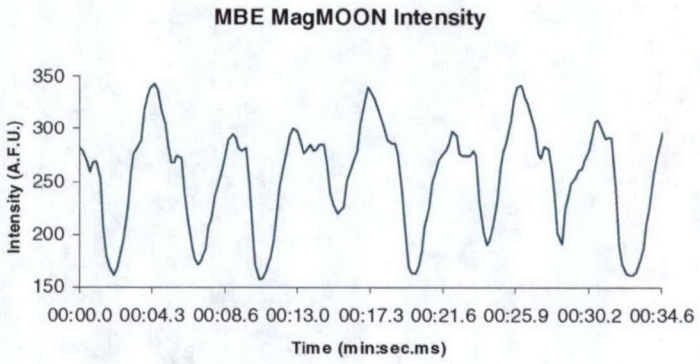

Figure 10. Time series of fluorescence intensity from a 3.4 μm cobalt coated MagMOON rotated by a 0.25 Hz magnetic driving field.

We have also produced silica nanospheres coated with a magnetic layer of iron covered with a protective layer of silver. These were observed also observed to rotate in rotating magnetic fields, and produce a modulated reflection signal.

d) Modulating fluorescence from a pH sensing microdrill

Disease is often manifest by deviations from normal chemical balances. For instance tumors have areas of high pH and low oxygen (hypoxic)[4]. In order to better understand the chemical profiles of diseases, and ultimately to diagnose and cure them, methods are needed to measure chemical concentrations in tissues. The use of fluorescence has been limited by autofluorescence and scattering from tissues, as well as a need to introduce fluorescent sensors to the area. We are developing a magnetically actuated drill that can pass through tissue and monitor chemical concentrations. The drill may also be designed to administer local hyperthermia or deliver drugs, and observe the chemical response *in situ.* By modulating fluorescence from the drill as it rotates, the background signal can be subtracted. Scattering can be accounted for by examining the spectral shape of the fluorescence emission. Previously Ishiyama *et al.* have shown that a similar drill can be guided in three dimensions using magnetic fields, and that it can drill through bovine tissue, although their drill lacked the ability to sense chemical concentrations[5].

A 2 mm screw was attached using epoxy glue to a 2x2x10 mm neodymium-iron-boron magnet magnetized through the diameter (Dexter magnets) in order to make a magnetically driven remote drill. The drill could propel through agarose gel and gelatin.

The drill was then coated by a thin fluorescent pH sensing layer. The coating was performed by dipping the screw part of the drill in a solution of 7 ml tetra-hydrafuran (THF), 40 mg of 6000Mw polyvinyl chloride (PVC), 100 µl of Nitrophenyl Octylaether (plasticizer) and 1 mg of the pH sensing dye choromionophore 3 (ETH 5350). This combination forms the basis for more sophisticated ion sensors where an ionophore is added to the matrix[1]. The screw was removed to allow the THF to evaporate and deposit a thin layer of pH sensing polystyrene film. Next, one section of the drill was coated with a layer of black ink applied with a Sharpie felt tip pen. The drill was driven into an gelatin solution with a rotating magnetic field, and then a series of spectra were taken with the drill rotated back and forth to the "on" and "off" positions. Subtracting "On" minus "Off" spectra clearly and reproducibly removed background signals. Figure 11 Illustrates the principle of the microdrill.

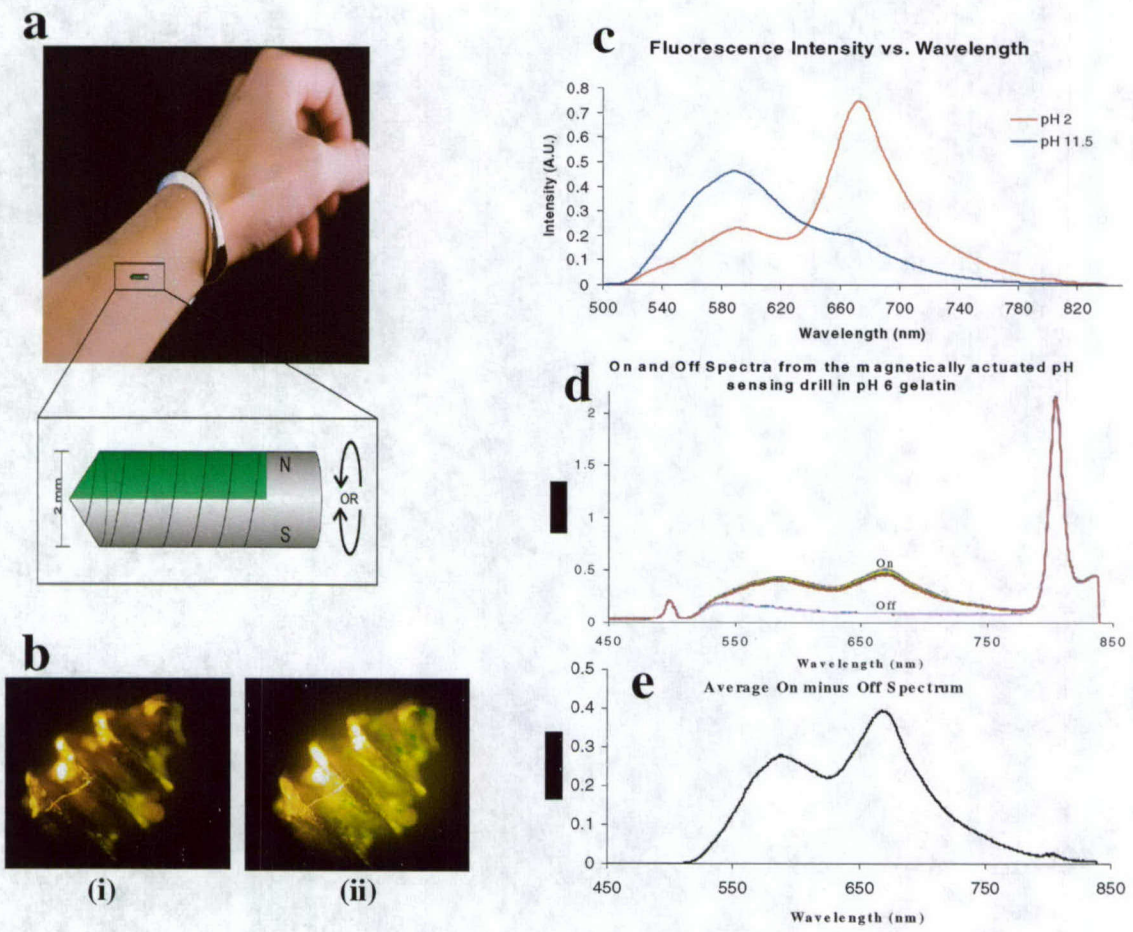

Figure 11. (a) Schematic of the principle (b) Images of a fluorescing microdrill, (i) bright field image, (ii) fluorescence and bright field image. (c) Spectrum of microdrill in acid and basic buffers. (d) Magnetic modulation "on" and "off" spectra. (e) "On" minus "off" subtracts off the background, and separates drill fluorescence from background.

e) Preparation of Brownian MagMOONs

A drop of a solution containing 1-2 µm fluorescent superparamagnetic polystyrene microspheres (Polysciences) in a water or ethanol-water mixture was spread out on a glass slide using a pipette tip, and allowed to dry to deposit a monolayer of nanospheres. The slide was then placed in an aluminum vapor deposition system and coated with approximately 100 nm of aluminum thereby capping the particles. Particles were removed with a damp paintbrush and suspended in water after 30 seconds of sonication. A small drop of the solution was placed on a slide and viewed under a microscope to confirm the yield of Brownian MagMOONs.

This technique was used to produce particles over a wide ranges sizes (50 nm – 3 um) and compositions (silica, polystyrene; superparamagnetic and non-magnetic). The fluorescence and reflection of the particles were observed to blink and rotate due to Brownian forces. The rotation rate depends on size and local viscosity. In addition, the blinking allows signal separation, similar to MagMOONs (see section II.d)

f) Fluorescence Enhancement from Reflective Metal Coating

Relatively thin coatings of aluminum and gold are reflective (skin depth is 9 nm for aluminum and 17 nm for gold for 589 nm light[6]). For large particles, classical optics applies, and metal capping can be used to focus and reflect light. For smaller particles, particle scattering allow observation of particles as small as 50 nm. In addition, local electric field enhancements and plasmon resonance properties of metallic nanoparticles create novel optical properties.

We recently discovered that metal capping enhances the fluorescence from microspheres. This is illustrated in Figures 12b and 12c, where 3.4 μm particles oriented towards the objective emit approximately 2.3 times more light than the adjacent uncapped microspheres. This enhancement arises from increased excitation path length as well as reflection towards the objective of fluorescence that would usually be emitted away from the objective. Observation of magnetic and Brownian motion of capped particles also indicates that the light is reflected directionally within the particle.

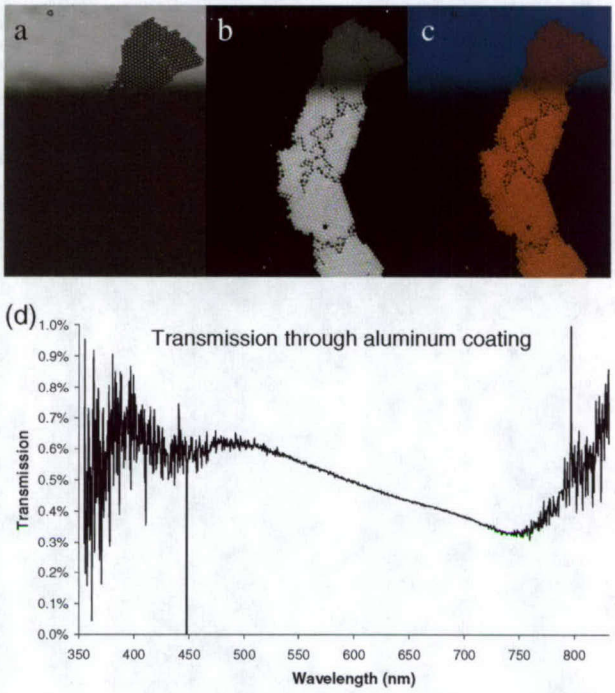

Figure 12. A monolayer aggregate of 3.4 μm microspheres with aluminum coating on the bottom ¾ of the view. (a) Bright field image at the edge of the metal coating with high transmission on the top where the metal coating is absent. (b) Fluorescence from coated particles (bottom) and uncoated particles (top). The metal coating results in higher intensity fluorescence. (c) Overlaid bright field and fluorescence image. (d) Transmission spectrum through the aluminum layer. The noise at high and low wavelengths is due to low signal from an incandescent lamp source. The coating thickness is estimated to be 50nm.

These enhancements are an important feature for obitical nanosensors, and motivated the development of other hybrid architectures such as strawberry and nanoprism-coated particles.

g) Magnetic Assembly of Strawberry-Shaped particles

Precisely controlling functional materials with well-defined shapes and dimensions on the micro/nano-meter scale is an important challenge for material science. Due to the interest in nanodevices and their unique electronic, magnetic, mechanical and optical properties, connecting and assembling functional components into a predefined pattern has been the focus of many investigations.[7-11] For example, strawberry-like composite materials using organic-inorganic hybrid particles might lead to unique applications in electronics, photonics, biochemical sensing, catalysis and "smart" materials.[12-17] Although polymerization techniques such as the emulsion copolymerization [13; 16]and intra-micellar polymerization [17] have been used before to prepare strawberry-like particles,

the complicated synthesis process, the tedious pre-treatment and their limitations to polymeric materials hamper these techniques widespread use, especially for inorganic materials such as metal or semiconductor particles. Thus the patterning of organic or inorganic spheres is an important and alternative method for the fabrication of strawberry-like spheres. An alternative approach using electrostatic, biological or non-covalent chemical forces for forming strawberry-like composites has also previously been utilized.[14; 15] However, an elaborate design of ligands or functional groups on the surface is a prerequisite, and binding reactions are slow when large (>500 nm) sized particles are used, due to their slow diffusion rates, especially at low particle concentrations.

To integrate particles into possible photonic or electronic devices, positioning multi-component particles with nano/submicron resolution is necessary. In technological systems, the magnetic dipolar interaction has served as a powerful tool for organizing one-dimensional chains or two-dimensional superstructures from spherical particles [18-24] with the help of external magnetic fields. To our knowledge, however, this technique has not been realized for creating multi-component patterns from micro/nanospheres [25; 26].

Here, a self-assembly method, based on magnetic attraction, giving strawberry-like particles with stable and precisely arranged microstructures, has been developed. Ferromagnetic nanocrystals (CrO_2) coated onto commercial polystyrene particles(PS) act as nanometer magnetic traps to confine paramagnetic colloidal particles. Controlling the properties of the two kinds of magnetic colloidal particles in solution, we found that they self-assembled into a strawberry-like structure, with substantial flexibility in the implementation of the chemical, optical and physical functionalities of both the core and the decorating spheres. Compared to conventional techniques, the magnetic force mediated self-assembly process reported on here has the following advantages. 1) This is a simple but effective technique for forming a strawberry-like microstructure; no pre-treatment or post-modification is necessary. 2) The magnetic attraction leads to rapid surface reactions between the particles. 3) This approach can be widely adapted to all organic and inorganic materials. 4) Desirable properties can be efficiently tailored by adjusting the concentration, size, and properties of the surface decorating and core particles according to the application. 5) Many different shapes of components, such as rods, cubes or pyramids, can be used as alternatives for spherical micro- or nano-particles. 6) A variety of treatments can be performed on the particles after they are assembled, including melting, adding additional

components, or selectively dissolving the magnetic components. Thus, the methodology demonstrated here gives a new, simple but powerful example for depositing and forming a variety of micro- or nano-building blocks.

Strawberry-shaped particles were magnetically assembled from large core particles and small decorating particles. The core particles consisted of polystyrene microspheres, 4-5 μm in diameter, coated with chromium dioxide nanorods, approximately 300 nm long and 50 nm in diameter (Spherotech Inc., Libertyville, IL). For some experiments, the core particles were functionalized with carboxyl groups on the surface; for other experiments, they were functionalized with biotin. A dilute solution of the core particles was magnetized in a 1000 G magnetic field, and smaller magnetic decorating particles were added. A wide range of magnetic decorating particles were used, including polystyrene nanospheres 200 nm to 1 μm in diameter (with carboxyl or SuperAvidin functionalization), and 200 magnetic silica nanospheres synthesized in our lab. Figure 13 illustrates the assembly of strawberry-shaped microparticles.

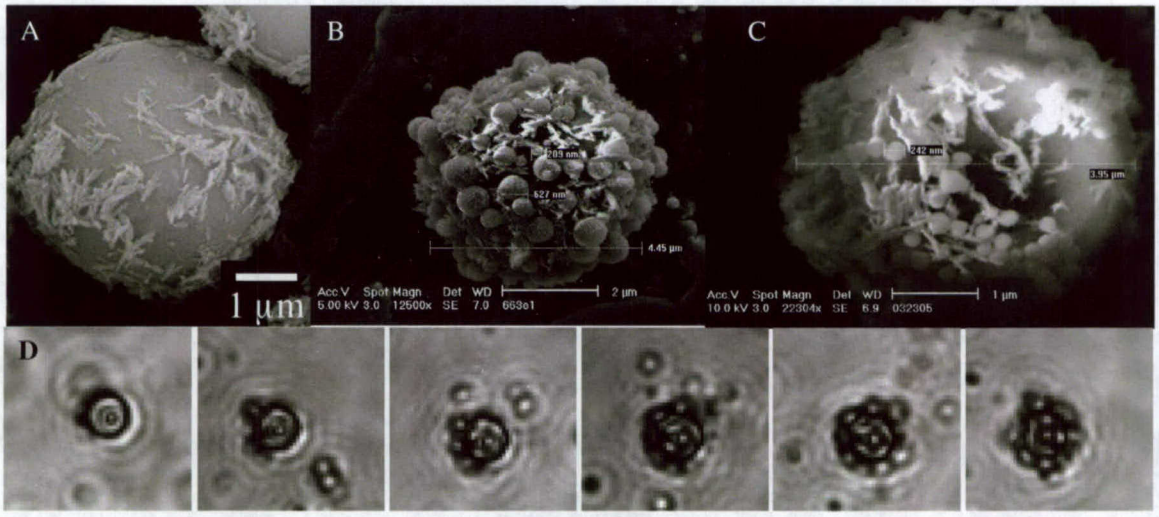

Figure 13. Magnetic assembly of strawberry-shaped particles. (A) An SEM image of a 4-5 μm permanent magnetic microsphere consisting of a polystyrene core coated with chromium dioxide nanorods (Spherotech, Inc.) (B) SEM image of a 4.5 μm permanent magnetic polystyrene core coated with 600 nm polystyrene particles. (C) SEM image of a 4.3 μm permanent magnetic core particle coated with 200 nm silica nanoparticles containing iron oxide, and synthesized in our lab. (D) Progression of brightfield images showing assembly of 0.86 μm superAvidin coated magnetic microspheres, (0.86 μm, solid 1%, binding capacity: 0.69 μg biotin-FITC/mg spheres) onto biotin coated ferromagnetic core particles, 4.32 μm (suspended in pH=7.4 PBS buffer).

h) Nanoprisms and Nanoprism Hybrids

We fabricated nanoparticle with novel architectures incorporating metallic nanoprisms on the surface of silica and polymer nanoparticles. Metallic nanoprisms are recently discovered particles with sharp facets that have interesting and controllable optical, chemical and electronic properties. The sharp edge of the triangle shape dramatically enhances the electric field at the tip, and can lead to enhanced optical coupling (antenna effect) as well as enhanced non-linear optical properties, especially when the particles are close to each other. We plan to fabricate prism-coated MagMOONs that combine these optical enhancements with magnetic modulation.

The Ag nanoprism colloid was chosen as the starting platform because of the colloid's interesting shape, and optical properties. Nanoprisms have dipole and quadrapole plasmon resonances present in their absorption spectrum. The plasmon resonances for the nanoprisms are sensitive to the edge length of the colloid, colloid thickness, and to the degree of truncation of the tips of the triangle (Figure 14). An increase in the edge length or a decrease in the thickness of the colloid will red shift the dipole plasmon resonance, while rounding or truncating the nanoprism tips will blue shift the dipole plasmon resonance by up to 50nm. This leads to a highly tunable colloid for biological sensing applications.

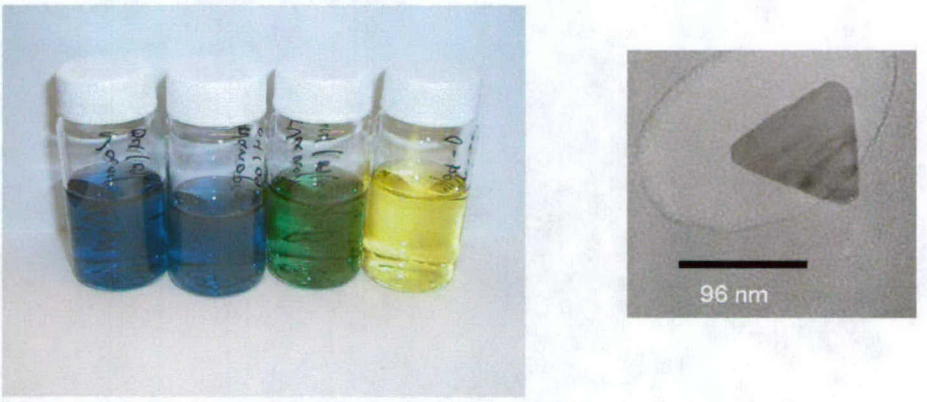

Figure 14. a) Controlling the size of silver prisms allows tuning of the plasmon resonance and hence solution color. b) TEM image of a single silver nanoprism for a solution with blue color.

In synthetic work performed to date, Transmission Electron Microscopy (TEM) images show that the silver nanoprism particle size is very polydisperse for the current reaction conditions[16]. No literature has yet been found that records the attachment or

embedding of nanoprism colloids to functionalized ceramic particles. Preliminary work shows that it is possible to adapt the silica-Ag/Au core-shell procedure for the synthesis of ceramic-nanoprism core-shell nanoparticles (see Figures 15-17).

Figure 15. A suspension of silica nanosphere coated with blue nanoprisms that are beginning to sediment. Note that colloidal solutions of prisms do not sediment and are difficult to separate from solution.

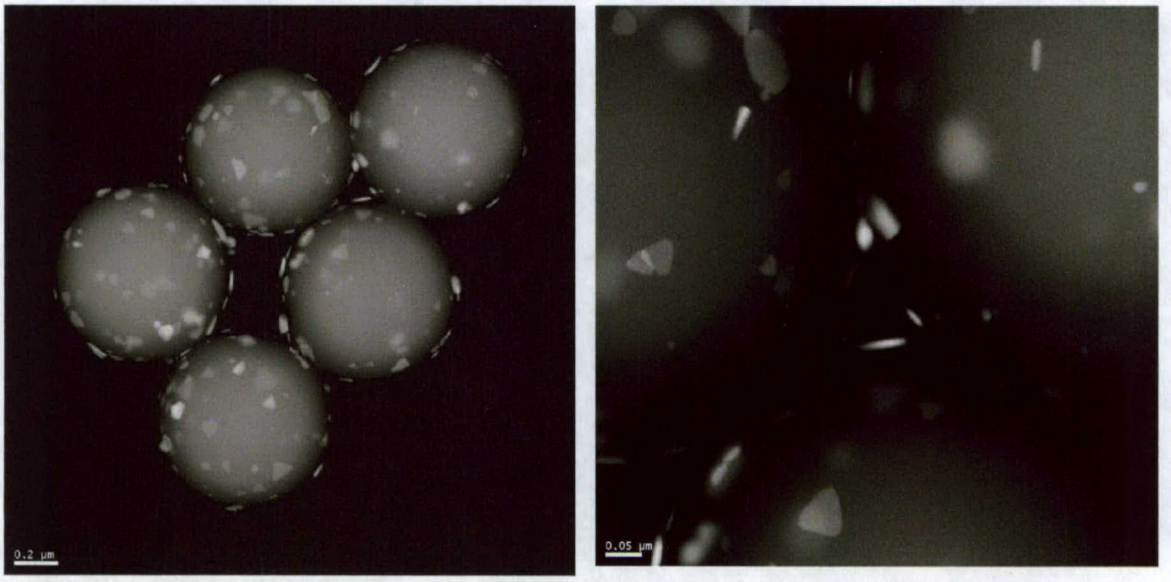

Figure 16. High-angle angular dark-field STEM images of nanoprisms assembled onto 970 nm silica nanospheres. The large number of prisms per sphere, and coupling between spheres holds promise for single sphere SERS chemical detection.

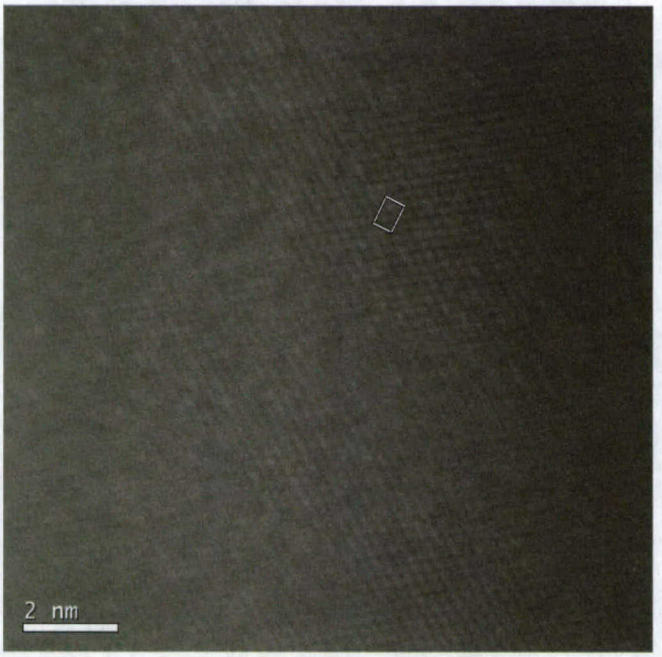

Figure 17. High-resolution STEM of a silver nanoprism on the surface of a silica nanosphere. The image shows the 110 crystal facet; individual lattice planes on the atomically flat surface are visible. The lattice spacing is the same as bulk silver.

A promising use of the prism coated MagMOONs is for Surface Enhanced Raman Spectroscopy (SERS). Raman spectroscopy has several advantages over fluorescence spectroscopy. At room temperature, Raman spectra are much sharper than fluorescence spectra, allowing better identification of analytes such as hormones, dissolved gases, DNA, and explosives. The sharp spectra also allow many analytes to be detected simultaneously without spectral overlap. In addition, bleaching is far less of a problem for Raman spectroscopy than for fluorescence spectroscopy. The main limitation of Raman spectroscopy is that Raman signals are approximately 10^{14} times weaker than fluorescence, so Raman signals are often drowned out by background fluorescence. Analytes that adsorb onto the surface of certain "hot" metal nanoparticles have a SERS signal 10^{14} to 10^{15} times greater than signal in solution, making the Raman signal similar in magnitude to fluorescence (Nie and Emery. Science. 1997; 275(5303):1102-1106). However, such "hot" particles are rare occurrences, and fluorescent backgrounds are still a problem. By loading hundreds of nanoprisms onto each MagMOON, there is a greater probability of having a "hot" particle. In addition, the coupling between particles is expected to enhancement the SERS effect.

We have fabricated the first nanoprism-covered silica nanoparticles and are exploring their optical properties. The particles hold promise for the detection of native biochemicals in living cells[27], detection of explosives, and disease diagnosis. In addition, by providing a method of concentrating and separating the nanoprisms from solution without precipitating them, the hybrid particles may have applications for catalysis, chemical extractions and non-bleaching dyes.

Certain applications may warrant aspherical core geometry such as a pancake or roll shape[28; 29]. Polystyrene microspheres approximately 3um in diameter can be flattened into pancake shapes using a small rolling pin. In this process the 3um polystyrene spheres are placed on a microscope slide by drop coating. Then a nanoprism suspension, or labeled cytochrome c solution is added dropwise, and the particles are rolled together using the rolling pin. This process should work well for this application, because work has already been performed rolling nanoparticles of different compositions together into polystyrene pancake shaped structures. The smaller nanoprism colloid particles will act as "nano-crumbs", and coat the larger micron sized particle that is being flattened into a pancake structure.

i) Fabrication of Biodegradable Polyacrylamide Nanoparticles

We have synthesized magnetic nanoparticles and targeted magnetic nanoparticles. However, for *in vivo* use of nanoparticles for imaging or therapeutic purpose, toxicity is one of the most important factors. This toxicity includes not only the toxicity of materials but also easy clearance from the body after use. Nanoparticles larger than 20 nm will not be cleared from the body easily. To overcome the problem of clearance, we are developing biodegradable polyacrylamide nanoparticles. These acrylamide nanoparticles are formed using a biodegradable crosslinker, glycerol dimethacrylate, and increasing the amount of initiator to make the degraded polyacrylamide chain smaller. The degradation of nanoparticles, synthesized with 35% crosslinker and suspended in Phosphate Buffered Saline (PBS) at 37 °C, were monitored with time by Gel Permeation Chromatography as in Figure 18 below. The peak shift toward the right (longer retention time, i.e., low molecular weight) shows that the nanoparticles were degraded with time in PBS. The synthetic protocol for nanoparticles is given in the Table 1 below.

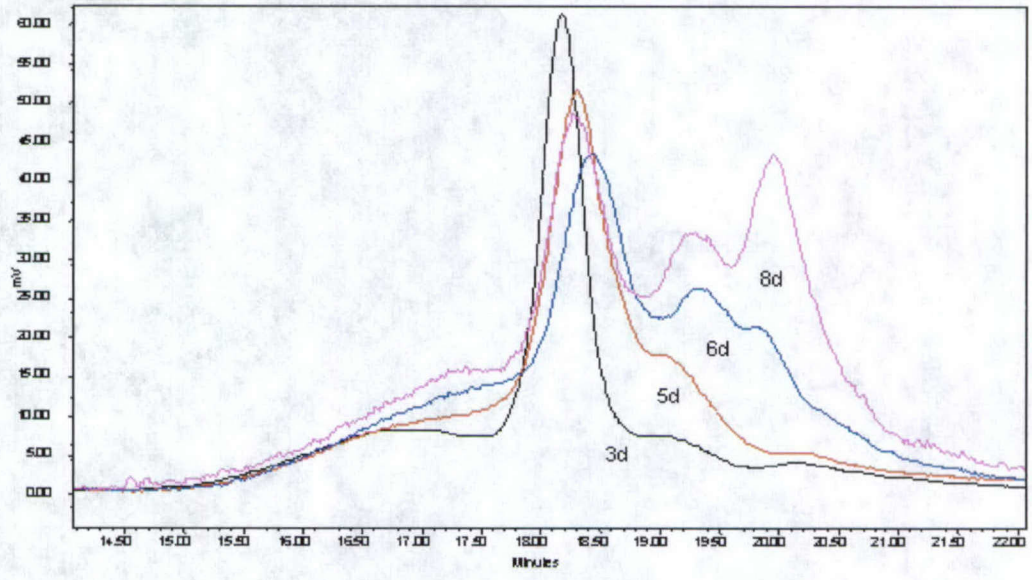

Figure 18. Biodegradation of nanoparticles in PBS, measured by gel permeation chromatography as a function of number of days (d) in solution.

Table 1: Synthesis Protocol for biodegradable acrylamide nanoparticles

Acrylamide	0.25g
Glycerol dimethacrylate	0.5g (85%)
AOT	1.6g
Brij 30	3.2g
Hexane	43ml
Methanol	3ml
Sonication	Clear solution
Argon	30min
TEMED	10ul
Ammonium persulfate (400ug/ul)	500ul
Temperature	Room Temp
Reaction Time	Overnight

j) Development of Electric Field Nanoprobes

In addition to MagMOON chemical probes, and nanoviscometers, we are developing probes to map electric fields in complex microenvironments such as tissues. Ideally, these measurements should be performed with point probes that do not perturb the field under observation. Optical nanoscale probes come very close to this ideal. We have recently developed optical nano-sensors that occupy minimal volumes and are electrically neutral (Buck, 2004) thus inducing minimal electrical interference while measuring specific ion concentrations. However, no such nanoscale device has yet been made for the measurement of electric fields.

As an example of a voltage nanosensor, the hydrophobic voltage dye, di-4-ANEPPS was embedded inside an organically modified silica (ormosil) nanosensor about 100nm in diameter. The nanosensors were placed in an optical cell (125μm thick) between two electrodes, and the emission spectrum was recorded when varying voltages were applied across the cell. The PEBBLE fluorescence was excited between 350-500 nm (Olympus blue dichroic mirror unit). A preliminary calibration is shown, based on taking the emission ratio of 534 nm and 670 nm. Figure 19 shows fluorescence spectra, for these voltage PEBBLEs, in 0 field and at a high field of 7.9×10^5 V/m. It should be noted that the fluorescence came from the particle rather than the free dye. These results provide proof of principle for the operation of the voltage dye nano-probe.

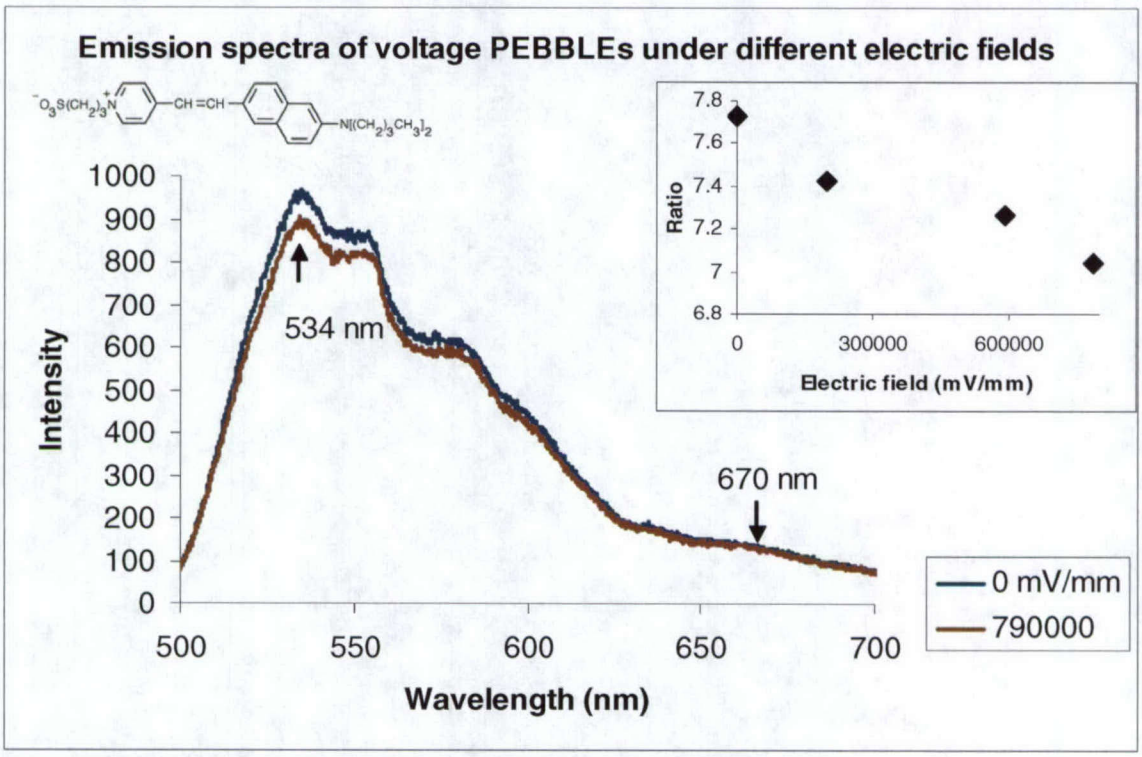

Figure 19. Voltage nanosensors containing di-4-ANEPPS dye (formula shown above) in 100 nm ormosil PEBBLEs. The nano-sensors are calibrated on a micro-spectrometer by varying the electric field while exciting the nanosensors between 350-500 nm (Olympus blue dichroic mirror unit) and taking the emission ratio of 534 nm and 670 nm. The inserted graph is a preliminary calibration of the nanosensors; the ratio decreases as the electric field increases. The molecular formula of the voltage dye is given at the top.

Although voltage dye PEBBLEs work well for measuring high fields, they are not sensitive enough to measure low fields. This limitation arises because the sensing mechanism involves the motion of only about one charge across the dye's length. In order to measure low fields, new probes must be developed that measure the cooperative motion of thousands of charges over distances closer to a micron. This is possible by measuring the orientation and rotation rate of "electroMOONs" with permanent electric dipoles. The dipoles are produced by attaching different charge groups to the two faces of moon-shaped particles.

II. Instrumentation, Techniques, and Applications

Most fluorescent nanospheres and microspheres emit light uniformly in all directions and have spherically uniform chemical and physical properties. Coating polymer nanospheres with a metal hemisphere shell breaks this symmetry and gives the particles new optical[30; 31], chemical[32-34], electrical[32; 35], and other physical properties. Controlling the optical symmetry of particles produces new tools for the exploration of optical, chemical, and materials properties of surrounding environments. They can be used as nano-instruments such as: nanoviscometers[36-41], nanothermometers[42], nanobarometers, and nano-chemical sensors[1; 2; 43-47]. Modulation of Brownian MOONs and MagMOONs also allows the local optical, chemical, and materials properties to be distinguished from the bulk properties. These novel tools promise intracellular chemical imaging with improved signal over background, high sensitivity immunoassays with simpler procedures, measurements of viscosities at chosen time and size scales, observation of micro-vorticity in fluids, and simultaneous intracellular physical and chemical imaging.

During the project, we enhanced our capabilities for MagMOON fabrication, while improving our instrumentation and expanding the techniques and applications for MagMOON sensors. We assembled a CCD imaging setup for imaging MagMOONs and Brownian MagMOONs, using reflection or fluorescence to observe rotation from individual particles (down to 50 nm with reflection). We wrote software to analyze the motion and infer viscosity and particle size. We developed a model to describe signal to noise ratios for various situations. We showed that MagMOONs could be modulated in a conventional plate-reader. We also showed proof of principle for MagMOON and Brownian MOON viscometers, friction probes, particle sizers, intracellular biomechanical probes, and roving modulated light sources. These nanotools hold promise for chemical, biomedical, and materials research. Figure 20 shows applications being explored for MOON particles.

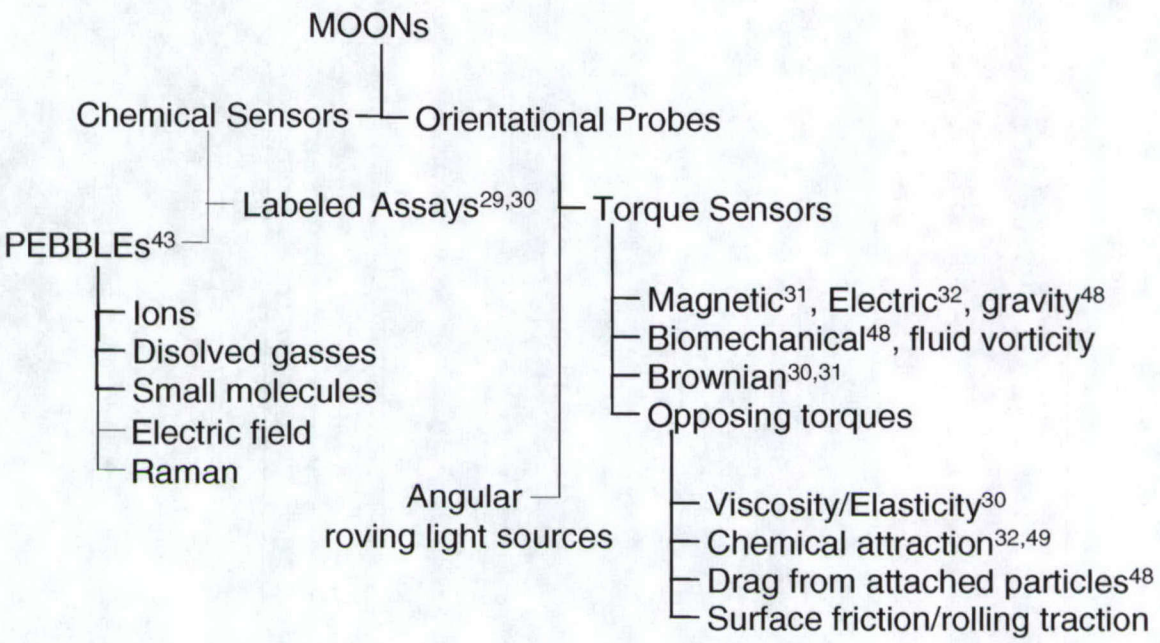

Figure 20. Applications being explored for MagMOONs and Brownian MOONs.

a) Instrumental Setup

i) CCD Setup

We assembled a new CCD setup to acquire streams of images of MagMOONs and Brownian MagMOONs on our microscope. The system works in brightfield, epifluorescence, or reflection mode. A computer controlled wavelength switcher can rapidly switch the excitation wavelength in order to provide ratiometric images for chemical imaging using fluorescent dyes and MagMOON sensors.

We wrote computer scripts to analyze the image time series in order to measure particle rotation rate, and infer the torques acting on the MOONs. Tracking particle orientation reveals the torques acting on the particle, from sources including: electrical fields[32; 35], magnetic fields[31], gravity[48], Brownian forces[30], biomechanical forces in macrophages[48], chemical attraction[32; 49], fluid vorticity, translation/rotation coupling, and the opposing torque of the medium's viscous drag and elasticity.[30] All particles in view are tracked simultaneously allowing measurements of individual particles, ensembles, and spatial maps.[31; 48; 50]

ii) Reflection

We also expanded our imaging capabilities from fluorescence to reflection, by using a 50% beam splitter in place of a fluorescence cube. Reflection from metal coatings on MagMOONs provides a strong signal, and allows the visualization of individual nanospheres (down to 50nm). The signal is modulated when the particles rotate under magnetic, Brownian, and other torques. In addition the signal doesn't bleach, and a wide range of wavelengths can be selected, including red and infrared wavelengths where artifacts from scattering are minimized. The reflection signal can also be used as a reference for ratiometric fluorescence chemical sensing, although in the current setup, measurements are sequential rather than simultaneous.

The use of smaller particles allows us to probe over a wider range of size scales, from size scales on the order of viruses and vesicles to mitochondria and nuclei to whole cells. Smaller particles are more sensitive to small changes in size caused by biodegradation, adsorption of proteins or pathogens, or biomechanical forces.

iii) Assay Setup

Just prior to the start of the grant, we showed proof of principle for MagMOON immunoassays. We used aluminum capped 4-5μm Streptavidin coated magnetic particles to measure the relative concentration of Oregon green labeled biotin and Phycoerythrin labeled biotin. The experiment demonstrated that magnetic modulation could be used to separate the MagMOON spectrum from background signals from autofluorescence, excess label not attached to the particles, and electronic backgrounds. The assay itself was a competition between two fluorescently labeled analytes, demonstrating that MagMOONs can be used in competitive assay formats, and also in ratiometric chemical detection schemes. The fact that unattached dye is not affected by magnetic fields and forms part of the background leads to simplified washing procedures that will be useful for the development of portable field instruments. MagMOON assays also may also be used for dyes that bind only weakly, where washing excess label off would interfere with the experiment. The assays were performed using metal capped MagMOONs[31] and aspherical MagMOONs[29].

Since then we improved the setup, using electromagnets to modulate the signal, directly measuring weak fluorescence from streptavidin, and using nanoparticle binding to enhance

the signal. In addition, to observing MagMOON modulation using a microscope and spectrometer, we also used a commercial plate reader.

Modification of Microwell to allow magnetic Modulation of MagMOONs

MagMOON based assays offer a number of advantages over conventional assays such as ELISA. They also offer much higher sensitivity than purely magnetic assays and use standard components. This leads to simple modifications of current instruments, or development of portable instruments designed specifically to take advantage of MagMOONs. Adding an electromagnet (an open coil of wire with current passing through it) to a microwell would enable magnetic modulation of MagMOONs within the wells by changing the direction of the current in the coil. This simple modification allows currently available microplate readers to perform accurate background subtraction without requiring any changes to the reader hardware.

Figure 21 shows an example of a microwell modified for magnetic modulation. Copper wire was wrapped 30 times around a thin tube of plastic that was inserted into a microwell on a standard 96 well microwell plate. The plastic tube was made from a section cut out of a 1 ml pipette tip. A solution of 4-5μm MagMOONs as described above was added to the microwell. A small positive current was passed through the coil and created a field that oriented all metal-capped MagMOONs in a solution in the well "on." A small negative current oriented all MagMOONs in the well "off." With no current, the particles all aligned with the remnant field in the room, and were oriented in a phase of the moon closer to "on" than "off." This example demonstrates that a simple inexpensive modification of existing microwells will allow standard plate readers to read "on" and "off" signals from MagMOONs in solution without any moving parts. The simple construction also lends itself to portable instruments for fieldwork using robust and inexpensive electronic components (LEDs, photodiods and electronic filters) with no moving parts.

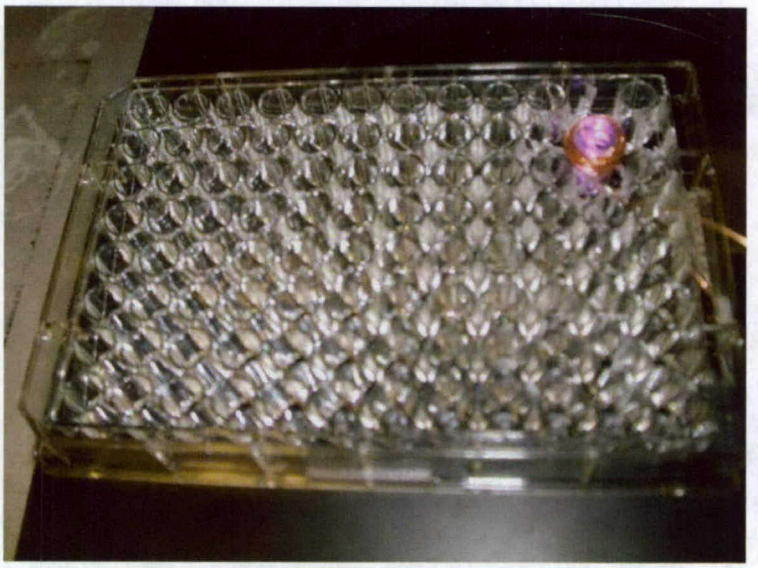

Figure 21. Photograph of a 96 well microplate with an electromagnetic coil inserted into one of the wells to modulate fluorescence from MagMOONs in the well.

Direct Measurement of Streptavidin Fluorescence on MagMOONs

Many analytes of interest fluoresce under blue or ultraviolet excitation. However, large background signals common at these excitations limits sensitivity of direct fluorescent measurements in the ultraviolet. Instead, sandwich assays and competitive assays are performed using intense visibly excited dyes. However, addition of fluorescent labels complicates the procedure (especially if unattached labels need to be removed). A direct fluorescence measurement technique may facilitate instruments for portable field tests.

We have shown that the intrinsic fluorescence of streptavidin can be separated from background signals using magnetic modulation of streptavidin coated metal-capped MagMOONs. Streptavidin coated 4-5 μm ferromagnetic particles (Spherotech Inc., Libertyville IL) were capped with aluminum, suspended in a solution of deionized water, and modulated by orienting them "on" and "off" in magnetic fields. A fluorescent spectrum from the weakly fluorescing Streptavidin directly linked to the particles was detected. This weak signal contrasted with no detectable signal from a control (similar particles without Streptavidin), and strong fluorescent signals from Streptavin that had been fluorescently labeled with biotin linked fluorophores (Figure 22).

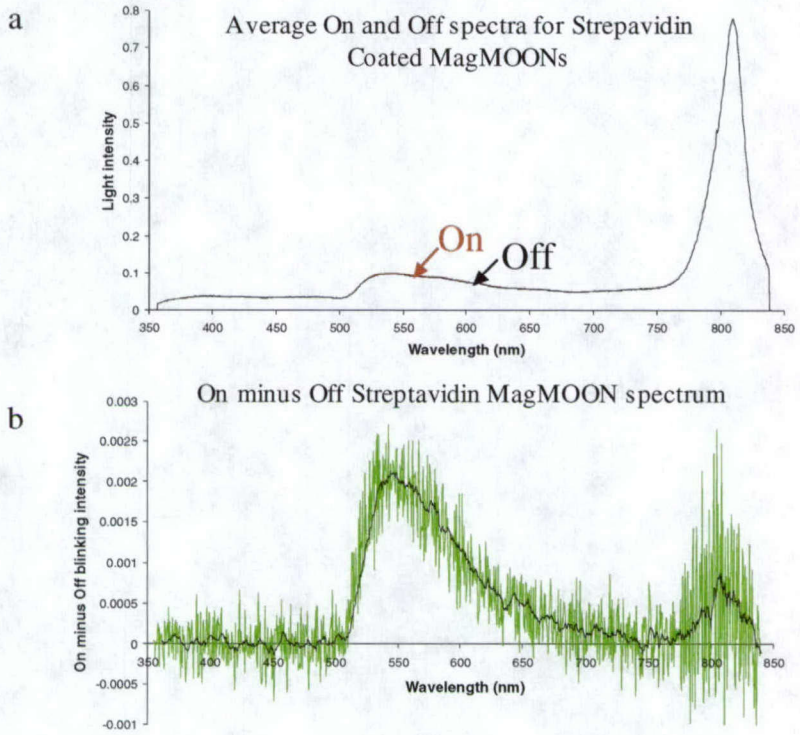

Figure 22. (a) Average On (red) and Off (black) spectrum from a Streptavidin coated MagMOON. (b) On minus Off MagMOON spectrum reduces 800 nm mercury lamp background by a factor of a thousand (principal components analysis, see report section d, further improves separation). The green is the subtracted spectrum, the black line is a smoothed spectrum.

Plate Reader Setup

In one MagMOON immunoassay scheme, the MagMOON acts as a substrate onto which fluorescent labels attach in the presence of analytes. This scheme uses the same reagents as conventional immunoassays, except that the substrate is a suspended MagMOON instead of a labeled microtiter plate. Potential advantages of MagMOONs include: 1) More sensitive measurements for plates with large variations in background, 2) Homogenous, mix and measure format where no washing is required, "dirty" samples can be used, and reactions can be followed in real time leading to information about binding rates in varying conditions. Such binding rate information is of fundamental interest in biomedical, and drug screening tests, and may also be used to improve immunoassay specificity by varying the conditions to attach and detach specific analytes (by varying pH for instance).

To test whether immunoassays could be performed on a conventional plate reader, we raised a Molecular Devices plate reader on wooden blocks, placed a magnet underneath, and rotated the magnet by hand to turn the MagMOONs "on" and "off." Figure 23 shows a photograph of the setup.

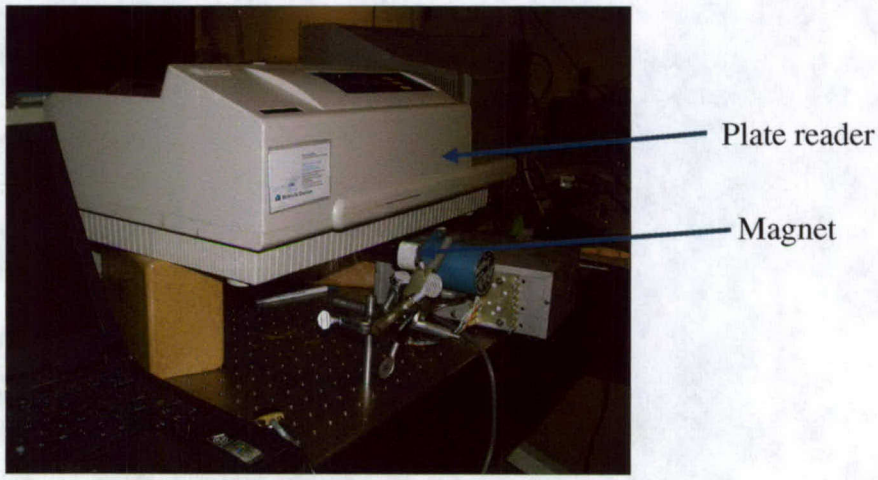

Figure 23. A setup using a magnet to modulate fluorescence from MagMOONs in a conventional fluorescence plate-reader.

The plate reader read all wells sequentially, and paused before acquiring a new reading in a time-series. During each pause, the magnet was rotated by hand by 180 degrees to flip the orientation of the MagMOONs in the plate. Figure 24 shows a time series for 12 wells with varying concentrations of fluorescent MagMOONs. A number of observations are evident: 1) The MagMOONs in all wells were modulated at each magnetic rotation, and the MOON signal could be separated from background (background was added in other experiments to demonstrate this). 2) The modulation is partial, not fully on to fully off: "off"

is 60% of "On." Use of an electromagnet, or proper magnet placement, is expected to improve the signal modulation. 3) There is variation in the average background level. The amount of variation was different from plate to plate, especially when fluorescent samples were used, but typically was ~10% of the background level 4) Noise was present, in addition to MagMOON modulation and background variation.

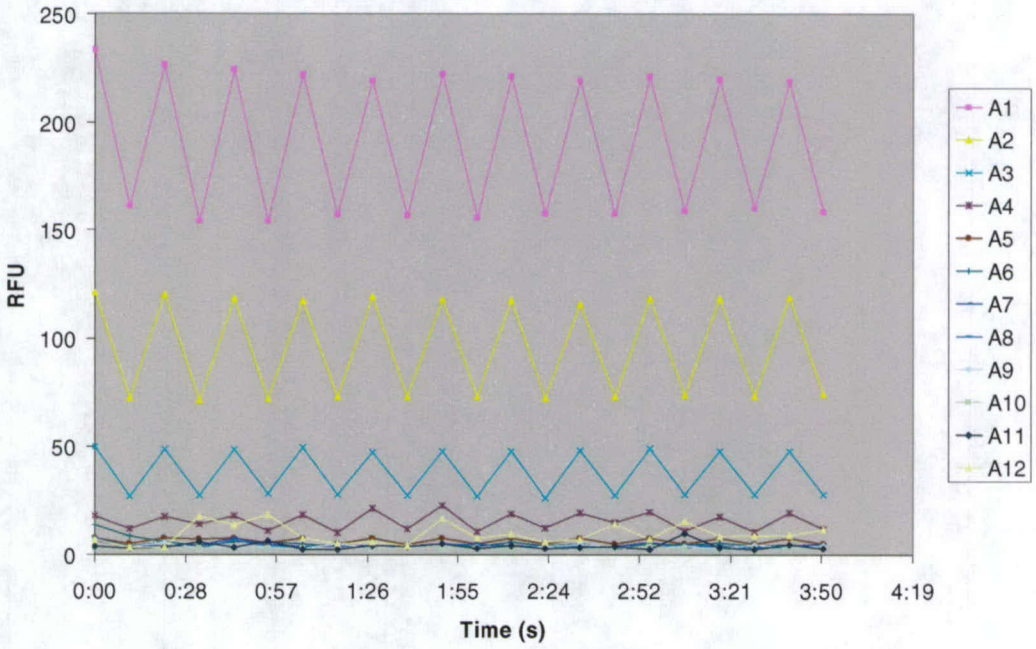

Figure 24. MagMOON modulation measured with a plate reader for decreasing concentrations of MagMOONs in wells A1-12.

In order to determine the theoretical sensitivity limitation for a homogenous MagMOON assay on the plate reader, we measured the noise as a function of fluorescence intensity (Figure 25 below). For weak signals, the noise was ~5% of the background, while for strong signals, the noise is ~1% of the signal, and increases linearly with signal strength. This noise would limit the dynamic range of MagMOON immunoassays acquired on this instrument to two orders of magnitude, unless very long time averages were used. According to the manufacturer, this noise is probably lamp fluctuation. It is possible to correct for lamp fluctuations by measuring the lamp intensity at the same time as acquiring the fluorescence intensity, however, another plate reader model would be required. Experiments using our more sensitive and controllable CCD microscope setup are ongoing.

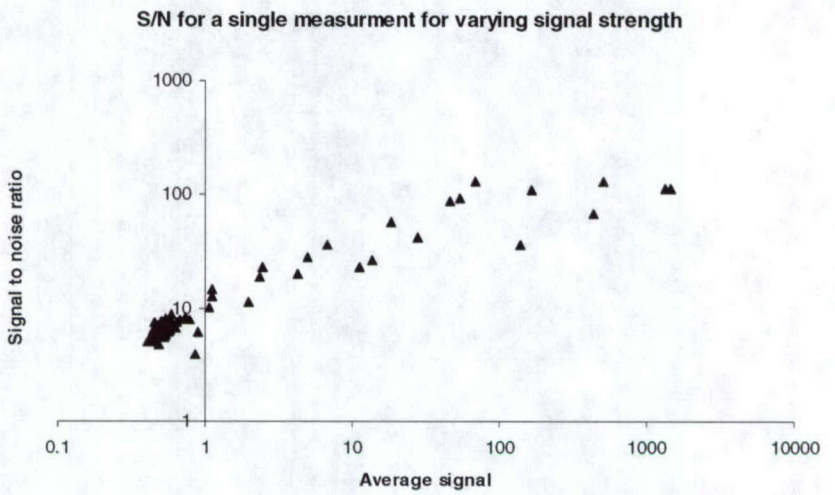

Figure 25. Signal to Noise ratio (S/N) for varying signal strengths. For more readings, S/N increases with the square root of the number of readings. The noise does not include uncertainty due to variation in background.

b) Signal and Noise Model

We developed a simple model to describe the signal to noise advantage for MagMOONs in various systems. MagMOONs reduce background interference from constant backgrounds, or background noise that varies at different frequencies. In addition, the modulation rate can be controlled to avoid noise distributed at specific frequencies (e.g. 60Hz). Background signals at other frequencies need not be discarded, as they can reveal information about the system. However, there are some types of noise such as shot noise, and read noise that occur at all frequencies and limit the signal to noise ratio for MagMOONs. In addition, noise from fluctuation in excitation lamp intensity can interfere with measurements, unless one simultaneously measures and corrects the excitation intensity fluctuations.

Optical sources from fluorescence, absorption, or reflection, generally produce strong signals: even single fluorophores emit 10^4-10^5 photons per molecule before photobleaching, and more with oxygen depleted samples. Reflection from metal-capped particles is stronger yet. With good optical setups >10% of these photons can readily be captured and converted into electrical signal.

Careful optical techniques rely on preparing a similar blank and subtracting background signals. Uncertainty in these background levels often limits measurement

sensitivity. This background variation becomes significant compared to random sources of noise when the background signal is strong, and/or long acquisitions and many pixels are averaged. In many biological samples and "dirty" samples, background may vary between 1-100% from sample to sample, or at different locations and times within a sample.

Uncertainty comes from a variety of sources including read noise, photon shot noise, dark current noise (electron shot noise), 1/f noise, and uncertainty in background. Equation 1 shows the average signal to noise level for a CCD detector model:

$$\frac{Signal}{Noise} = \frac{St}{\sqrt{R^2 + (B + D + S)t + (\alpha B t)^2}} \qquad \text{Equation 1}$$

Where S is the intensity of the signal of interest (in electrons read by the CCD), t is exposure time, R is read noise, B is the optical background intensity, D is dark current (electronic background intensity), and α is the percentage variation in background from sample to sample. The signal to noise ratio is reduced by a further factor of $1/\sqrt{2}$ if a blank with the same uncertainty is subtracted. The intensity of the signal ($S \cdot t$) and background ($B \cdot t$) depend on the exposure time, illumination intensity, optical setup, the sample properties, and the detector specifications. For a given setup, and illumination , ($S \cdot t$) and ($B \cdot t$) depend only on exposure time and signal to background level, although increasing excitation intensity, or changing setup can generally substitute for increasing exposure time. Averaging the values from many pixels, or averaging over many images or spectra may also substitute for increasing exposure time, provided the signal is sufficiently intense that read noise is not significant.

Figure 26 shows the calculated signal to noise ratios as a function of exposure time for a variety of typical signal to background levels, and for background uncertainties of 10%, and 0%. At low exposure times, read noise is the main source of uncertainty, and the signal to noise ratio increases linearly with t. At higher exposure times or stronger signals, photon and electron shot noise is the most significant source of uncertainty, and the signal to noise ratio increases with $t^{1/2}$. For strong signals, the signal to noise ratio is limited to the uncertainty caused by variation in background. Using MagMOON modulation for *in situ* background subtraction removes this uncertainty, making measurements more reliable in samples with small signal to background ratios or large variations in background.

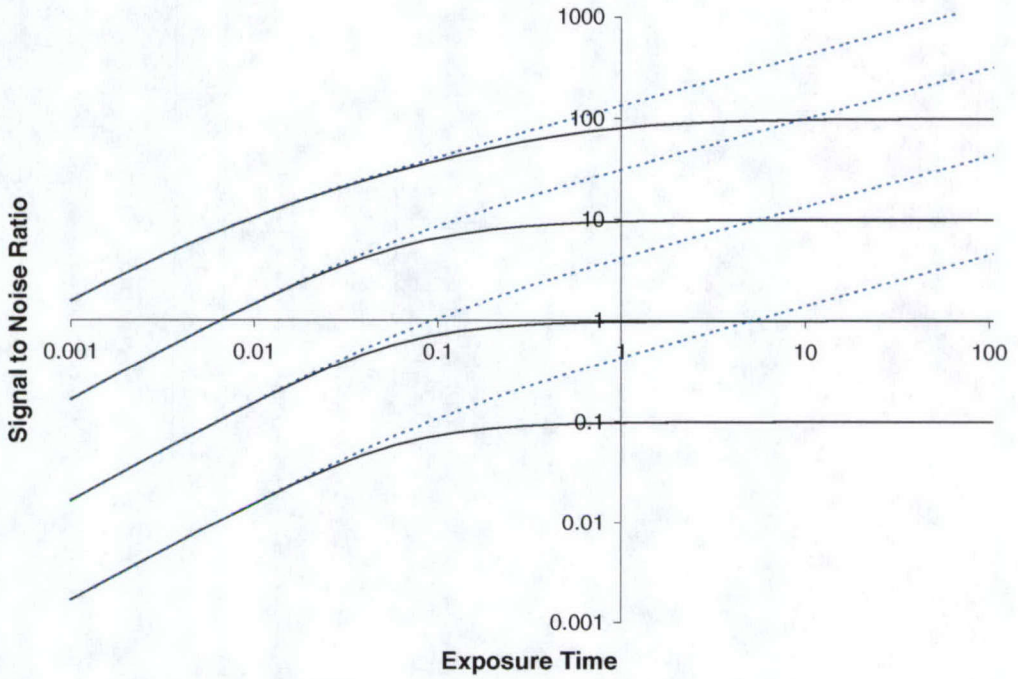

Figure 26. Signal to noise ratio for various exposure times and signal to background levels. Calculations are for a case with B=2000 electrons, R=12, D=4, and α=10% uncertainty in background level from sample to sample or in position and time within a sample (solid line), and 0% with MagMOONs (dotted line). Curves are plotted for S/B=10, 1, 0.1, and 0.01. The advantage of *in situ* background subtraction becomes more pronounced when variation is large and S·t is large. For reference, our Roper Coolsnap ES imaging CCD has a saturation of ~12,000 electrons/pixel (or twice that for a gain of 0.5), and a read noise of ~6electrons/pixel. There are typically a large number of pixels, and image frames or spectral acquisitions that can be averaged to improve signal to noise levels for MagMOONs. Such averaging increases signal to noise ratios by the square root of the number of averages.

MagMOONs also enable homogeneous mix-and-measure assays, where excess label remains in solution and particle signal is indistinguishable from the background except with magnetic modulation. Such homogeneous assays are limited in dynamic range to the maximum signal-to-noise ratio for a given exposure time (e.g. given a signal to noise ratio of 100 for a certain exposure time, a signal of <1% will be indistinguishable from noise, thus the dynamic range is ~100).

MagMOON Micro and NanoViscometers, Particle Sizers, and Magnetic Characterizers

Rotational viscosity is a fundamental property of materials relevant to fields from biophysics to materials and chemical processing. Its measurement is important for understanding molecular behavior, cell function, colloidal properties and bulk materials. For non-Newtonian and heterogeneous fluids, the measured viscosity is a complex function of

timescales over which forces are applied, and the size scale of the instrument used to probe the viscosity[38]. On the microscopic scale, measurements of viscosity in the cell cytosol have varied over six orders of magnitude depending on the size of the probe used[51]. Recent work suggests sieve-like structures within subdomains of cytoplasm that allow small particles to diffuse through while resisting the motion of larger particles[52]. In addition, liquid filled structures such as endosomes may allow particles to rotate within but not translate, causing divergence between rotational and translational Brownian diffusion. Macroscopic instruments determine viscosity by measuring the resistance of a fluid to mechanical movement. The same principle applies a microscopic scale, where magnetic forces can be used to torque MagMOONs, and the individual response of the MagMOONs to the driving fields is observed.[53]

In the low Reynold's numbers regime, MagMOONs rotate at a terminal angular velocity driven by the magnetic torque. The magnetic torque and equal opposing viscous drag are described by equations 1 and 2 respectively.

$$T_{mag} \approx MB\sin(\omega t - \theta)$$ Equation 2

$$T_{drag} \approx \eta V \dot{\theta}$$ Equation 3

Where M is the magnitude of the MagMOON's magnetic moment (remnance magnetization after magnetizing), B is the magnitude of the external magnetic field, ω is the driving frequency of the rotating external magnetic field, θ is the angle between the external field and the MagMOON moment, η is the medium's viscosity, and V is the volume of the MagMOON.

For slow magnet rotation rates, the MagMOON follows the external magnet with a small phase lag. As the rotation rate increases, the phase lag increases. Maximum magnetic torque and MagMOON terminal velocity occurs when the external magnet is perpendicular to the MagMOON's magnetic moment. At higher driving frequencies, the MagMOON is lapped by the external magnetic field resulting in a rocking motion at the frequency of the driving field superimposed on a slower overall rotation rate. Figure 27 shows the intensity time series from a single 4.4um fluorescent MagMOON in 88% glycerol (122 times more viscous than water) driven by a 1 Hz field, and below the same particle undergoing rocking and slow rotation with a 2.5 Hz driving field.

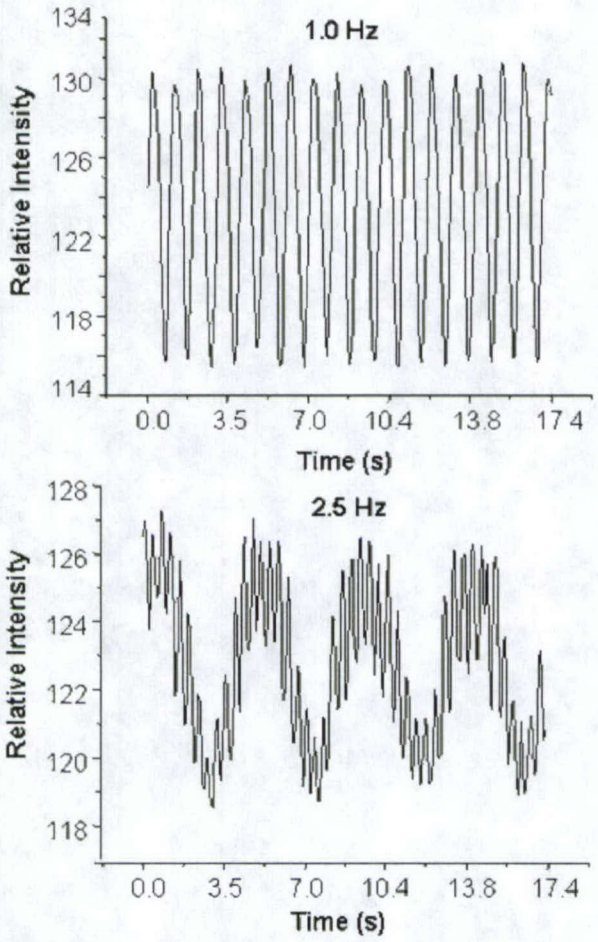

Figure 27. a) A 4.4 micron MagMOON orienting in a magnetic field rotating at 1.0 Hz. b) Slow rotation of the same MagMOON in a magnetic field rotating at 2.5 Hz.

The particle shape, external magnet field strength, particle volume, particle magnetization, and medium viscosity and elasticity or friction experienced determine the particles response, the phase lag, and the rate of slow rotation rate. As a result, these properties determine the time and pattern for step-out. For particles of known size and morphology the time series reveals information about the visco-elastic properties of the medium. Conversely, if the medium is homogeneous, then the response of individual MagMOONs can be compiled into comparative statistics giving information about the size distribution, morphology, or interactions of MagMOONs, and if the viscosity is known, absolute measurements can be made. Even in an inhomogeneous medium, with inhomogeneous particles, the frequency response of each particle reveals information about the local environment.

A drop of glyercol (88% w/v) containing suspended MagMOONs was place on a microscope slide. The microscope slide was inverted so that the drop it hung downwards, and MagMOONs in the solution were imaged with an inverted epifluorescence microscope (Figure 28). A function generator was used to precisely control the rate of rotation of a stepper motor connected to a cylindrical magnet that was magnetized through it's diameter. In addition, the microscope slide was placed on a heated stage to control the temperature of the glycerol solution.

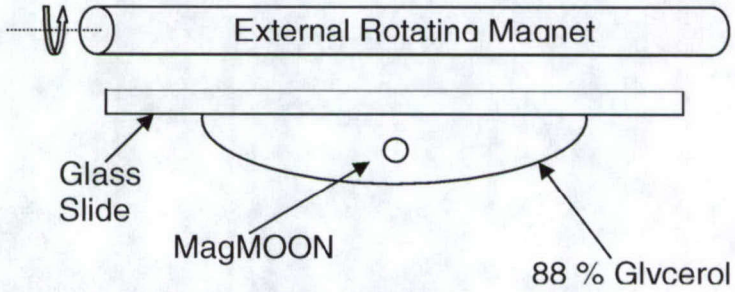

Figure 28. Schematic of the experimental setup for the MagMOON and glycerol solution.

The motor was rotated at a series of rotation rates, while the MagMOON fluorescence intensity was recorded with a CCD camera and analyzed with Metamoph Imaging software (Universal Imaging Corp.) It was found that there were two regimes for the behavior: at slow speeds, the MagMOONs rotated at the rate of the driving fields; above a maximum rotation rate, however, the MagMOONs underwent a rocking motion superimposed on a slow net rotation (Figure 27). Near the maximum rotation rate, the net slow rotation is very sensitive to slight changes. This is behavior matched well with the fit to the theoretical model for average rotation rate in a continuously rotated magnetic field:

$$< d\theta / dt >= \begin{cases} \omega, & \omega < \omega_{max} \\ \omega - \sqrt{\omega^2 - \omega_{max}^2}, & \omega < \omega_{max} \end{cases} \qquad \text{Equation 1}$$

$$\omega_{max} = MB / \eta \kappa V \qquad \text{Equation 2}$$

Where <dθ/dt> is the average rotation rate for the MagMOON, ω is the frequency of the driving field, ω_{max} is the maximum rotation rate, M is the magnitude of the MagMOON's magnetic moment (remnance magnetization after magnetizing), B is the magnitude of the external magnetic field, ω is the driving frequency of the rotating external magnetic field, θ is

the angle between the external field and the MagMOON moment, η is the medium's rotational viscosity, V is the volume of the MagMOON, and κ is a shape factor (6 for a sphere). The maximum rotation rate was determined by increasing the driving field frequency until the MagMOONs were observed to get lapped by the magnet and rotate backwards, however other methods include but are not limited to measuring the phase delay compared to the driving field for $\omega < \omega_{max}$, measuring the frequency of the slow rotation rate and fitting to the curve, measuring the maximum rocking rotation rate, or using different driving waveforms such as step function rotations and fields that oscillate +/- 90°. Some use of the last two methods are more easily adapted to measure the viscosity and elasticity of the medium as a function of frequency.

To demonstrate that the maximum rotation rate of single MagMOONs responded to solution viscosity, the glycerol solution was heated from 25.4 °C to 40 °C. The increase in viscosity and decrease in maximum rotation rate in the higher temperature glycerol is evident in figure 29. Note that viscosity measurements and spectral modulation may also be made in flowing solution; we have also observed MagMOONs rotating and blinking in solutions of water that were evaporating and causing high local flow rates.

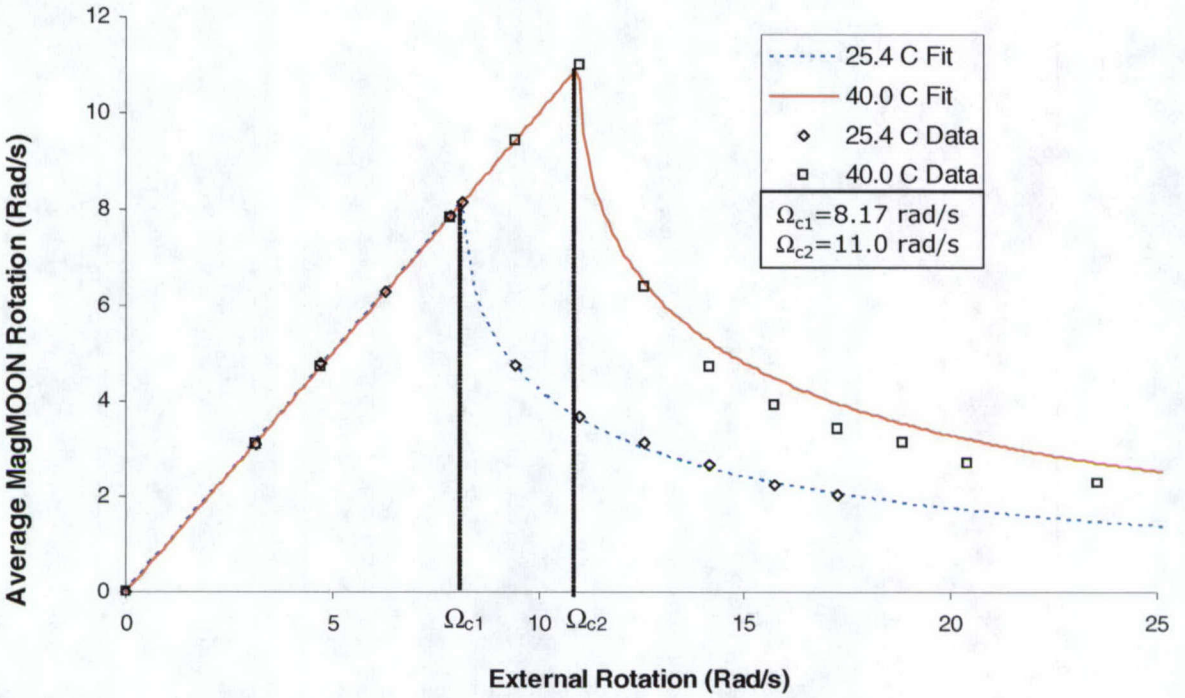

Figure 29. Average rotation rate as a function of driving frequency for a single MagMOON in an 88% glycerol solution at 25.4 °C and 40 °C.

MagMOONs also hold promise for measurement of binding. Based on current data with MagMOONs we can measure maximum rotation rate to better than 2.5%, and because it's a temporal based measurement, significantly higher sensitivity is possible. Indeed, using a 2.5% change in maximum rotation rate for a 4 μm particle corresponds to being able to detect a 33 nm increase in diameter or 17 nm in radius. Smaller particles (which may be formed using vapor deposition of magnetic material) are more sensitive to binding: a 1% change for a 400 nm particle corresponds to a 7 Å change in thickness across the particle surface, and with a 50 nm probes (preliminary results with Brownian MOONs indicate we can see particles down to this size), we should be able to see individual binding events for antibodies and measure the increased drag. The technique holds promise for measuring drag of molecules in solution, detecting binding equilibrium for individual molecules and particles, and detecting binding with viruses and bacteria. In addition the effects of binding are amplified if the binding affects the way the MagMOON chemically interacts with the surrounding medium (in the most extreme case binding to a surface).

c) Brownian MagMOONs

In the absence of external rotating magnetic fields, or for MOONs containing no magnetic material, the only surviving rotational motion of the MOONs is due to Brownian motion (rotation) as shown in figure 30b with fluorescence and 30d with reflection. This time series of intensity fluctuations contains information about the local rheology as well as information about the particle shape, size, and its interaction with its environment. Torques experienced by the particle and revealed by the blinking pattern include: viscous drag, elastic forces, binding interactions, gravitational torques, vorticity in fluid flow, and biomechanical forces. Magnetic modulation orients and rotates all particles synchronously, whereas for Brownian modulation, each particle rotates independently, unless they are physically attached (figure 31).

c) Brownian MagMOONs

In the absence of external rotating magnetic fields, or for MOONs containing no magnetic material, the only surviving rotational motion of the MOONs is due to Brownian motion (rotation) as shown in figure 30b with fluorescence and 30d with reflection. This time series of intensity fluctuations contains information about the local rheology as well as information about the particle shape, size, and its interaction with its environment. Torques experienced by the particle and revealed by the blinking pattern include: viscous drag, elastic forces, binding interactions, gravitational torques, vorticity in fluid flow, and biomechanical forces. Magnetic modulation orients and rotates all particles synchronously, whereas for Brownian modulation, each particle rotates independently, unless they are physically attached (figure 31).

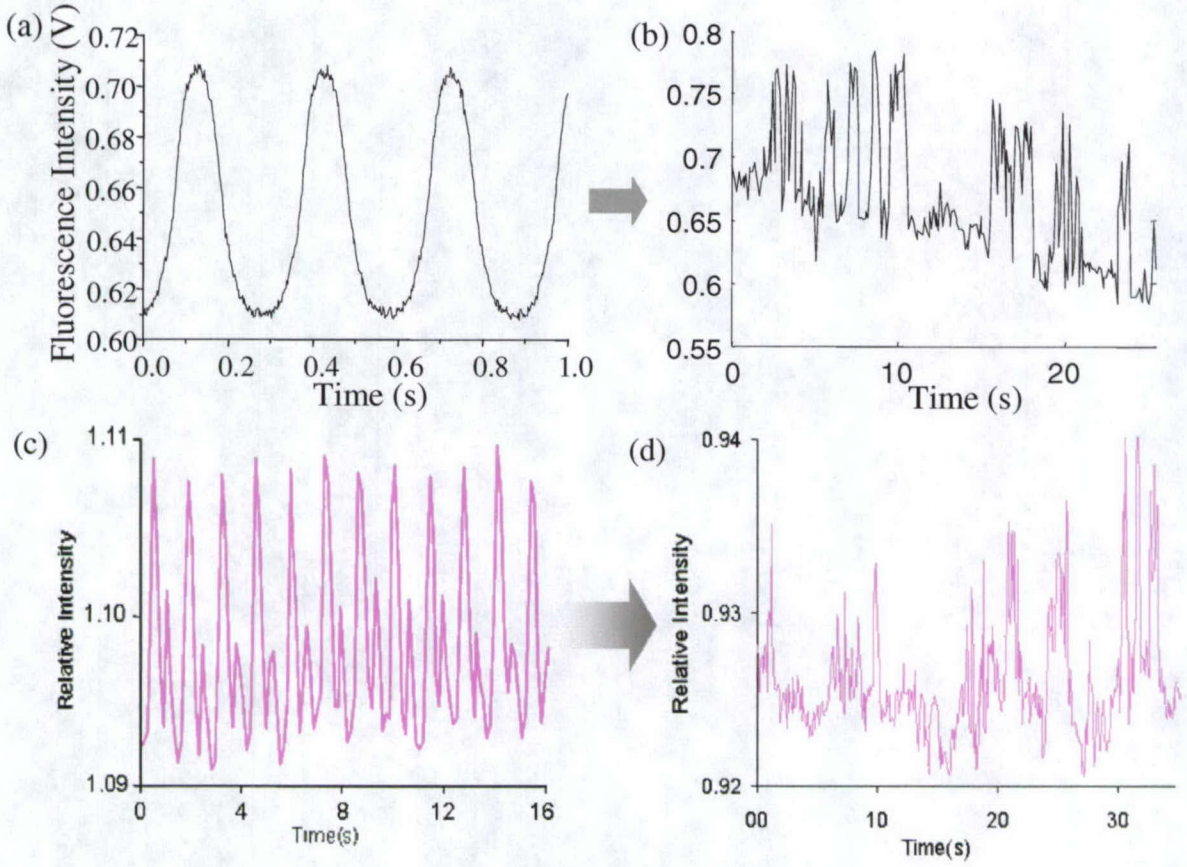

Figure 30. a) An ensemble of 4-5 μm fluorescent MagMOONs blinking at 3.3 Hz measured with a photodiode b) A single 2 μm Brownian MagMOON rotating in the absence of magnetic fields, measured with a spectrometer. c) Intensity time series for a single 4μm .reflecting MagMOON measured with an imaging CCD d) Reflected intensity timeseries for a single Brownian MOON on the order of 0.1 μm with aluminum coating in a viscous solution, measured with an imaging CCD.

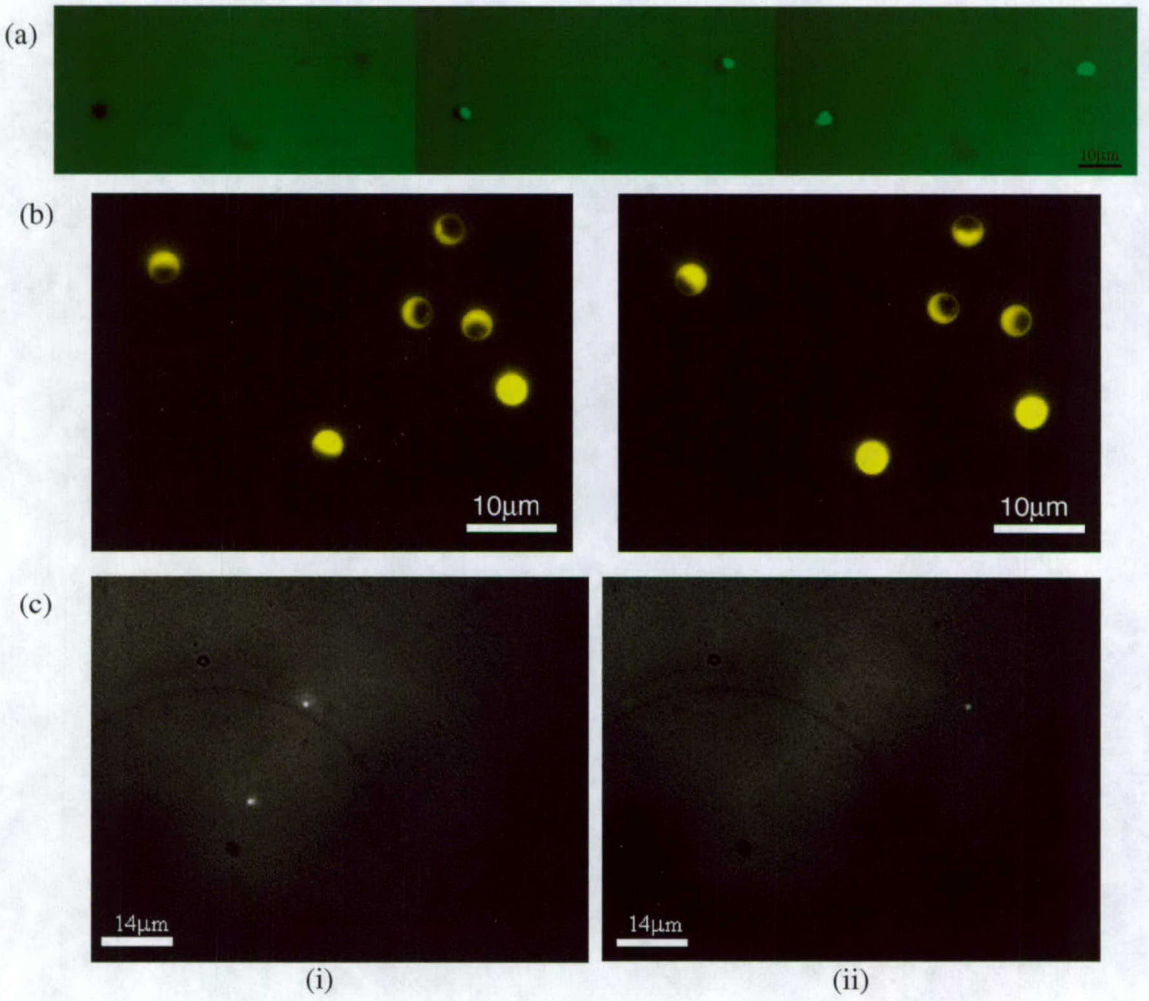

Figure 31. MagMOONs and Brownian MOONs, (a) 4.4 μm MagMOONs both oriented in the same direction by an external magnetic field. (b) Fluorescence from six different 3.4 μm aluminum capped Brownian MOONs individually rotating through the phases of the moon at two different times. (c) Reflection from diffraction limited 50 nm aluminum capped Brownian MOONs flickering on an off in a solution of 88% glycerol at two different times.

i) Separating the blinking Brownian MagMOON signal from other signals

A dilute solution of 1-2 μm fluorescent superparamagnetic Brownian MagMOONs prepared as described above was loaded into a rectangular capillary (Friedrich & Dimmock, inc.) by dipping the end of the capillary in the solution. The solution was viewed with an Olympus IMT2 epifluorescence microscope. One Brownian MagMOON moved into view, and a time series of 260 spectra were taken. A new spectrum in the time series was taken approximately once every 200 ms. Principal components analysis was then performed on the time series of spectra in order to separate out the different spectral components present in the spectra and to see how each component varied in time.

Figure 32a shows a time series of 250 fluorescence spectra consisting of a composite intensity at each wavelength from the following sources: intense mercury arc Lamp background, autofluorescence, room lights, fluorescent Brownian MagMOONs, one cosmic event or spike, and random electrical noise from the detectors readout amplifier.

Figure 32b illustrates that modulated particle fluorescence allows for separation of particle signal from the other sources as shown in the principal components representing the spectrum from each source: **(i)** Mercury lamp background and autofluorescence **(ii)** Brownian MagMOON dye 1 fluorescence **(iii)** Brownian MagMOON dye 2 fluorescence **(iv)** Cosmic spike **(v)** Spectrum of room lights **(vi)** the detector noise.

Fig. 32c shows the time signature for each of the principle components. The meaningful fluorescent signal from the Brownian MagMOON **(ii)** and **(iii)** has a distinct time signature from **(i)** the constant mercury arc lamp background and autofluorescence **(iv)** the cosmic spike at one instant in time **(v)** the decrease in roomlight entering through the door as the experimenter left the room and **(vi)** the high frequency hum of detector noise. The two dyes in the Brownian MagMOON had slightly different spatial distributions on the bright side of the Brownian MagMOON and also bleach at different rates.

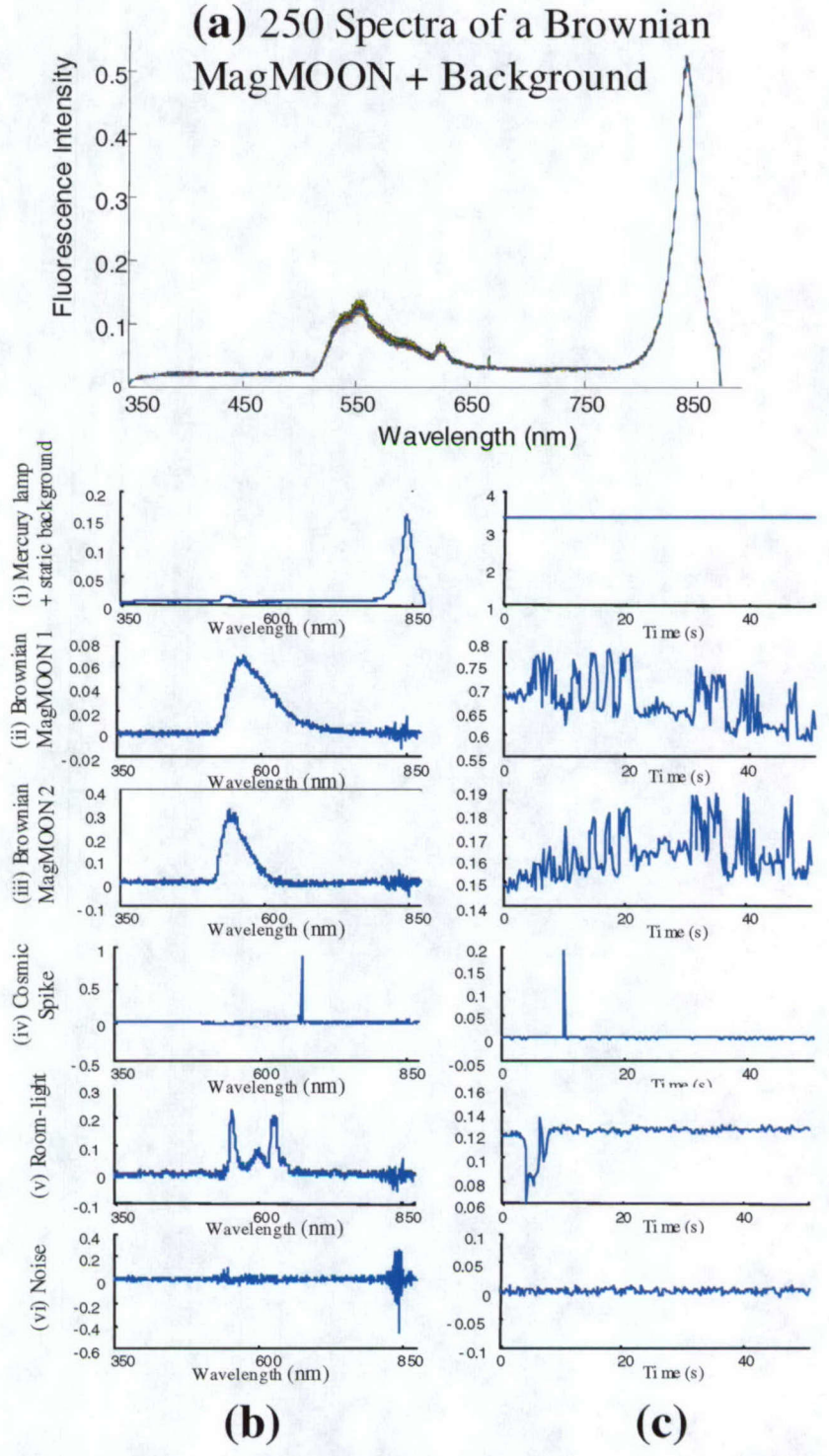

Figure 32. (a) 250 spectra from a Brownian MagMOON taken at 200 ms intervals. (b) Six spectral sources extracted from the time series above using principal components analysis (PCA). (c) The time series for each of the six spectra sources extracted using PCA.

By using Principal components analysis (PCA) to extract an erratically blinking signal from background, we have improved our already impressive ability to extract MagMOON signal from background. PCA also improved our ability to extract information from the background itself.

We discovered that the rate of Brownian MagMOON fluctuation is a measure of local rotational viscosity. Rotational viscosity is a fundamental property of any solution; in inhomogeneous and complex solutions, the viscosity depends on the size scale of the probe. Viscosity measurements within cells have varied over 6 orders of magnitude, depending on the technique and sized of the probe used[48]. On the 50 nm- 5 μm size scale, rotational viscosity is very difficult to measure with high spatial and temporal resolution by any other method. We expect that by measuring rotational viscosity within cells (or tissues), we may arrive at new insights into how cells work, and develop new diagnostic and research tools.

ii) MOON Viscometers

A time-series of spectra were taken of single 850 nm particles reorienting under Brownian motion. Usual data sets consisted of from 200 to 1000 spectra, recorded at 100ms or 200ms integration times, with no programmed delay between spectral acquisitions. Principle components analysis (PCA) was applied to the time-series in order to separate the Brownian MOON signal from other signals present in the spectra. In order to determine the rate of rotational diffusion, the autocorrelation function was calculated for the time series of the Brownian MOON fluctuations.

During the PCA, signals from Brownian MOONs are separated from the background, scattering, or other sources of fluorescence that may have an overlapping spectral emission. This signal separation dramatically improves signal to background levels. The main sources of light contributing to the observed spectra were determined using PCA and are shown in figure 33b. The time series, or "score," for each of the components in figure 33c is calculated by projection of the principal components onto the original data space[54; 55]. The random fluctuation rate for the Brownian MOONs, with a characteristic correlation time, τ_c is directly proportional to the rotational viscosity. Brownian MOONs thus provide a measurement of viscosity in their local environments.

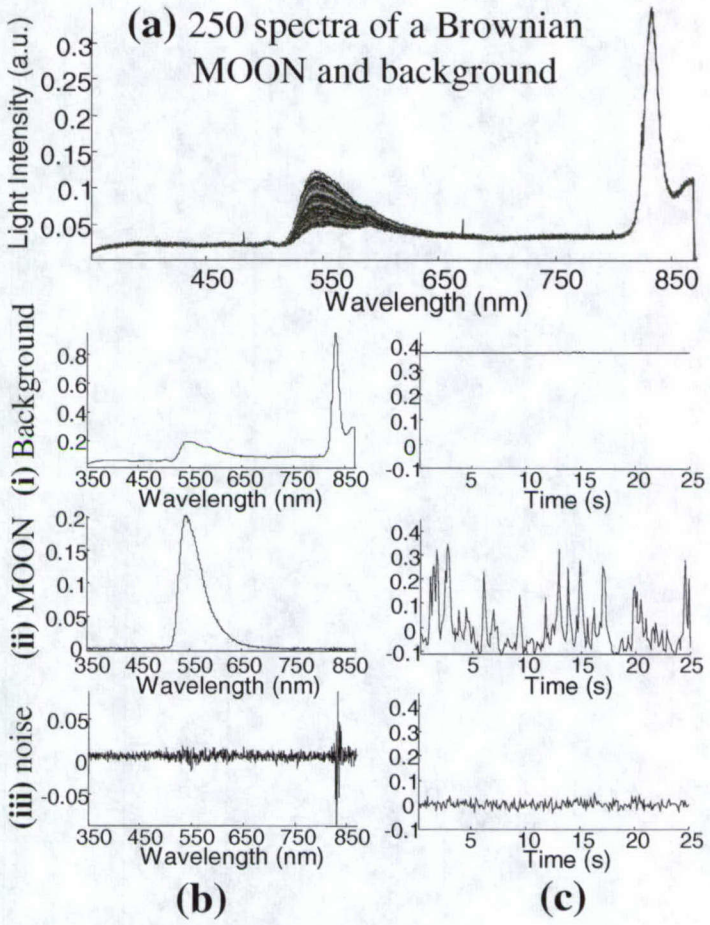

Figure 33. (a) Time series of 250 spectra containing multiple signals that vary in time. Shown in (b) are the spectra from the PCA with their corresponding time series shown in (c). Underlying spectra sources include (i) background fluorescence and mercury lamp reflection, (ii) Brownian MOON spectrum, (iii) noise.

The autocorrelation time for 850 nm aluminum coated Brownian MOONs in each solution was measured, and used to prepare the calibration curve shown in figure 34. Figure 34a shows typical autocorrelation functions from particles in different viscosity liquids. Figure 34b shows a calibration curve from the average autocorrelations for a number of particles and trials. The autocorrelation function decayed exponentially and, as expected, the decay rate increased linearly with increasing viscosity. Overall, the observed values for τ were systematically 25% shorter than predicted from theory. The theoretical values were calculated including the volume change from the 100nm aluminum capping (which increases τ by 18%) and the aspherical shape factor (which increased τ by 5%). Additional sources of

error include the presence of harmonics in the intensity dependence on angle which would decrease the observed τ. In addition, the viscosity of glycerol depends strongly on temperature and concentration, particularly at high glycerol concentration. At 68% glycerol and 24°C, a 1% change in glycerol concentration changes the viscosity by 10%, and an increase in temperature of 1°C decreases viscosity by 5%[56]. A100ms maximum acquisition rate for the spectrometer also limited our ability to detect fast changes in the fluorescence intensity at lower viscosities.

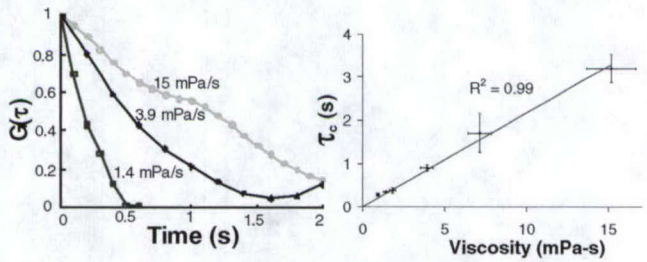

Figure 34. (a) Typical autocorrelation functions of the time series for particles in different viscosity solutions. (b) Average decay time, τ, of the autocorrelation function measured for a series of viscosities. The y-axis errors show the standard error for $\langle\tau\rangle$, while the x-axis error bars show a 10% error estimated from variation in particle volume and temperature variation. Viscosity was calculated from glycerol composition at 24°C[56].

iii) Rotation rate and Particle Sizing

In glycerol water solutions, viscous drag is the only significant torque damping the Brownian MOON fluctuations. The rotational diffusion equation predicts that, for short times, the mean square angular displacement increases linearly with time, according to the Einstein diffusion equation. As a result of the periodic boundary conditions, at 0° and 180°, the mean square angular displacement over a long time period exponentially approaches a maximum value. Experimentally, we calculate the mean square intensity fluctuation as $\langle\Delta I^2(\tau)\rangle = \langle[I(t+\tau)-I(t)]^2\rangle$, as a function of time lag,τ. Figure 35 shows $\langle\Delta I^2(\tau)\rangle$ resulting from rotational diffusion of nine different 850 nm Brownian MOONs in a 76% glycerol solution from the same image time series. Particle to particle variation in $\langle\Delta I^2(\tau)\rangle$ is small and arises from limited sampling time of the stochastic process. In addition, variations in particle size, angular intensity function, and particle environment also affect the autocorrelation function and should be measurable for longer acquisition times.

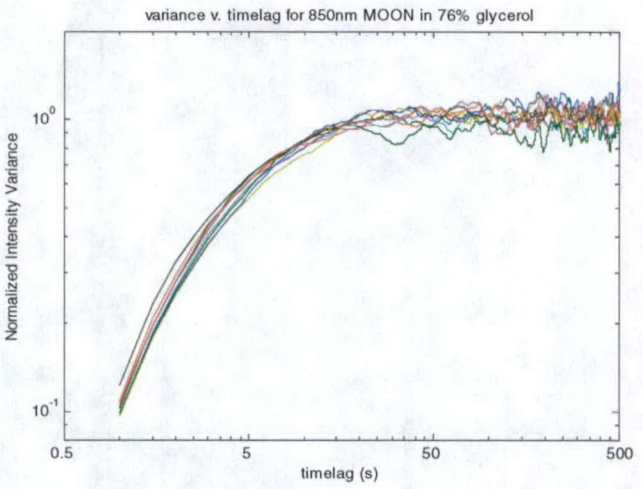

Figure 35. The mean squared intensity fluctuation (angular displacement) for nine 850 nm Brownian MOONs rotating simultaneously in a 76% glycerol solution at 24 °C. Note the log-log scale. Analysis used 4000 images acquired with a 500 ms delay between images.

The autocorrelation function also provides a measure of the angular diffusion rate. Figure 36 shows the mean autocorrelation function for several replicates of 300nm, 850nm, and 2μm Brownian MOONs in a 76% glycerol solution. The plot, presented on a semi-log scale, shows exponential decays with well separated time constants (time to decay to 1/e).

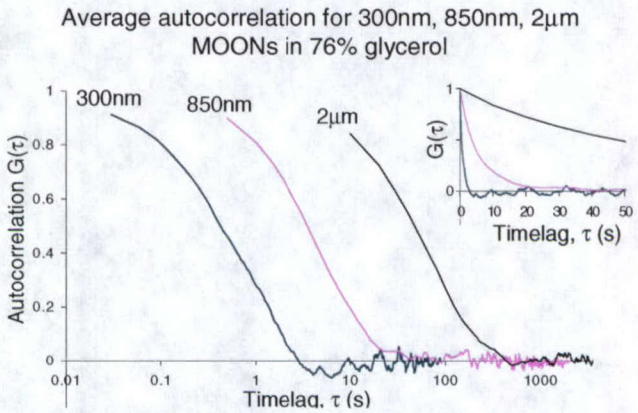

Figure 36. The autocorrelation functions for 300nm, 850 nm, and 2 micron Brownian MOONs with 50 nm Aluminum coating in 76% glycerol solution at 24 °C. Inset: same data-series plotted on linear axes.

iv) Particle Binding

At high particle concentrations, we are able to observe occasional interactions between particles and thus study the resulting aggregates. These aggregates can be directly observed for 2 μm particles, and inferred from the intensity rates for all particle sizes. Figure 37a shows the intensity fluctuations for a single 2 μm particle rotating in glycerol solution (top) and slower fluctuations for a single brighter particle (an aggregate) rotating in the same image series (bottom). Figure 37b shows the autocorrelation function for the aggregate as well as for ten single spherical 2 μm Brownian MOONs. The decay time for the aggregate is approximately twice the average decay time for the single particles.

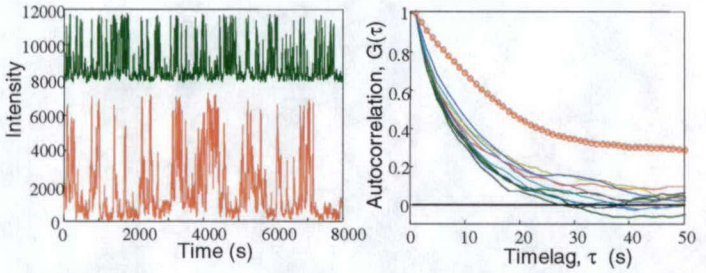

Figure 37. (a) The Intensity timeseries for a single 850 nm polystyrene MOON (green) positively offset for comparison with a dimer (red). (b) The solid lines show typical autocorrelation functions of a time series for ten single 850 nm Brownian MOONs with 50 nm aluminum coating in 56% glycerol solution at 24 °C. Shown with circles is the autocorrelation function for a dimer of 850 nm MOONs from the same image series.

The ability to measure rotation rates enables characterization of the drag on a MOON induced by binding, such as the binding of 50 nm viruses to 100 nm Brownian MOONs. Some of these applications require control over binding location relative to the capping material because the location of the binding affects the observed rotation rate. Control could be achieved by chemically binding or physically pressing ("breading") smaller particles into large particles before metal capping[7,][28][37] (figure 38)[29]. The same principle applies to measuring the maxiumum rotation rate of MagMOONs when particles bind to it. In addition to binding, tracking rotation rate may be used to study swelling and dissolving.

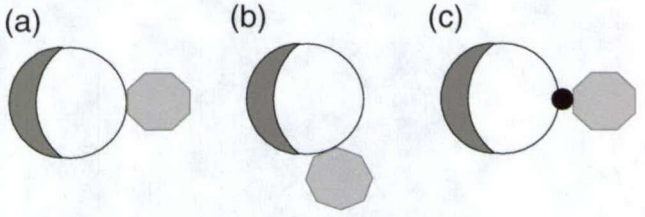

Figure 38. Schematic of a particle binding to a MOON. (a) and (b) show the particle binding to different locations on the MOON relative to the capping, creating different amounts of drag around the azimuthal axis. (c) Using local breading to control location of binding target.

v) Intensity-Angle Functions

Interpretation of intensity time fluctuations is limited by the approximations used to describe the fluorescence intensity of the MOONs as a function of angle. Modeling this function is difficult because it necessitates accounting for subwavelength scattering and absorption of excitation and emission wavelengths within the particle and from the metal capping. For instance, figure 6 illustrates that the metal capping enhances the fluorescence from the 3.4 μm MOONs observed at full moon phase. Intensity angle fluctuations obtained from rotating 4.4 μm MagMOONs indicate that the MagMOON intensity increases

monotonically with angle, that there is a first harmonic at about 1/3 the amplitude of the driving magnetic field rotation, and that they spend more time in dark phases than in bright phases. Brownian MOONs, with different sizes, with no absorbing magnetic material, and with different fluorescent dyes may have different angle intensity functions. In addition, particle shape and binding may also affect these functions.

Information about the angle intensity function is contained within the intensity time series. The top panel of figure 39 shows the intensity time series for a single 150 nm reflecting Brownian MOON. These MOONs flash "on" for brief periods, and spend most time in orientations closer to "off." A sort of the intensities in the series, the middle panel of figure 39, shows that approximately 270 of 300 intensities are relatively low. Assuming that all angular orientation states were visited with equal probability, and accounting for the differences in density of states at each azimuthal angle[48], the bottom panel of figure 39 shows the angle intensity function for the 150 nm particle. Included is the assumption that intensity increases monotonically with angle which may not be valid for reflecting particles because of reflection from both faces. This plot indicates that the intensity is weak for particle angles smaller then 140 degrees and increases rapidly for angles greater then 140 degrees. Longer acquisition times, and shorter exposure times give better defined characterizations. For two micron fluorescent Brownian MOONs this profile is much more gradual.[48]

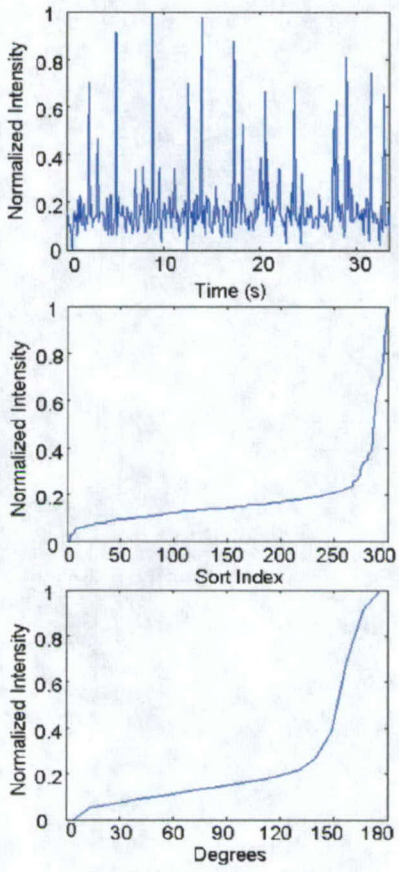

Figure 39: a.) Intensity time series for a 150 nm reflecting moon undergoing rotational diffusion. b) The sorted intensity values for the same 150 nm reflecting particle. c.) Angle intensity function assuming monotonic increase in intensity with angle.

Intracellular MOONs

In addition to studying particle interactions, Brownian MOONs can be used to probe environmental viscoelastic and biomechanical forces. Figures 40-42 show Brownian MOONs reorienting within macrophage endosomal compartments. This approach allows direct observation of endosome properties and torques on the endosome, on an individual particle and endosome basis.

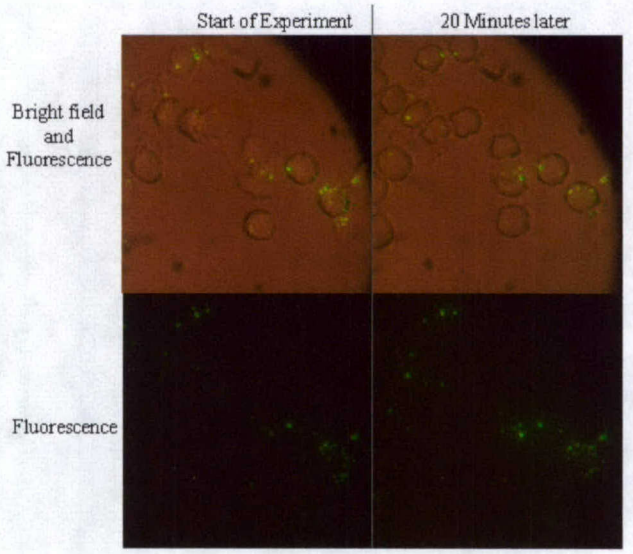

Figure 40. Brownian MOONs reorienting in macrophages. Top: overlaid bright field and fluorescence images showing Brownian MOONs internalized by rat macrophages at two different times, start of the experiment (left) and 20 minutes later (right). Bottom: Fluorescence images of Brownian MOONs reorienting in rat Macrophages.

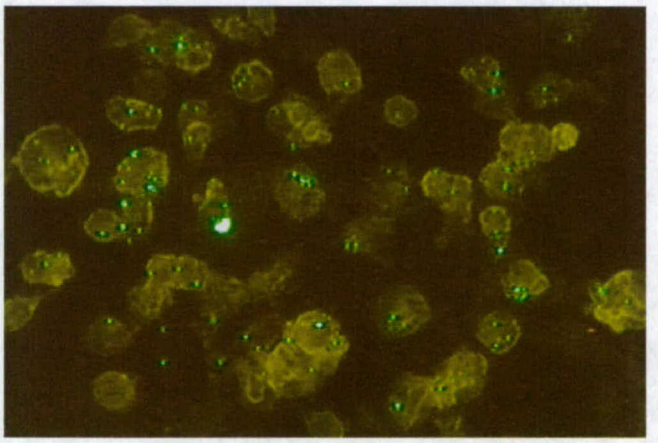

Figure 41. 300nm Brownian MOONs in endosomes within macrophages. Variation in intensity indicates MOON reorientation.

Figure 30 shows the fluorescence intensity from three 300 nm Brownian MOONs rotating and blinking in a macrophage due to biomechanical forces on the MOONs. The particles are actively translated and rotated at the same time. When the macrophages died, after ~20 minutes, the rotation stopped. Similar results were observed for Brownian MOONs in nearby cells. Combined with modulated chemical sensing this method is a tool for directly probing intracellular physiology and dynamics.

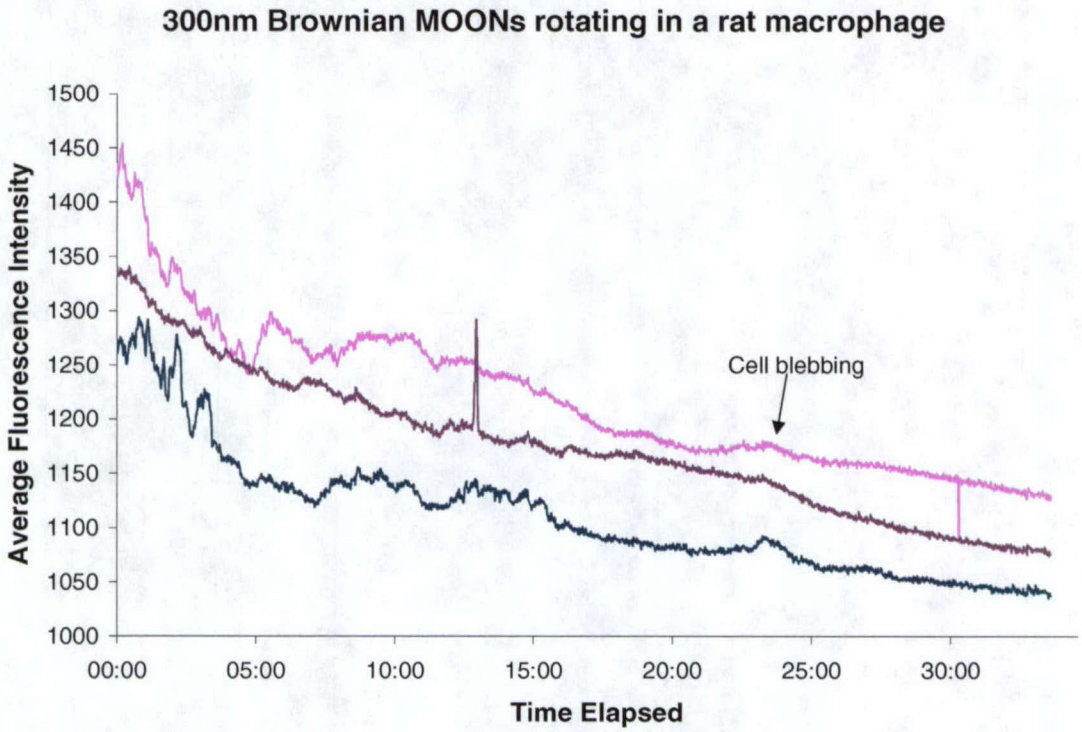

Figure 42. Blinking from three 300 nm Brownian MOONs in a rat macrophage rotating under biomechanical forces. The rotation slows and stops after the cell dies. Blue bleached the cell autofluorescence and the particles. The peak at 23 minutes is due to cell blebbing. The spike at 12:50 is due to a large Brownian MOON in solution passing nearby (see below).

f) Additional Applications of MOONs

i) Roving MOONlight

In addition to microviscometers, particles can serve as a modulated directional light source for angular illumination (roving moonlight) – a new form of imaging. Local illumination provides structural information in the vicinity of the probe, and could be combined with chemical sensing, for instance in studying stretch activated channels.[57] The orientation of the light can be controlled with an external magnetic field, or by allowing the particle to probe randomly under Brownian motion. Figure 43 shows an out of focus 2 μm Brownian MOON blinking and passing above a macrophage, during an experiment to measure rotation of 300 nm Brownian MOONs inside the macrophage (figure 30). Subtraction of two images, taken one second apart, removes constant background, and reveals an angular differential image. Positioning individual MagMOONs using our magnetic tweezer setup will provide more precise control.

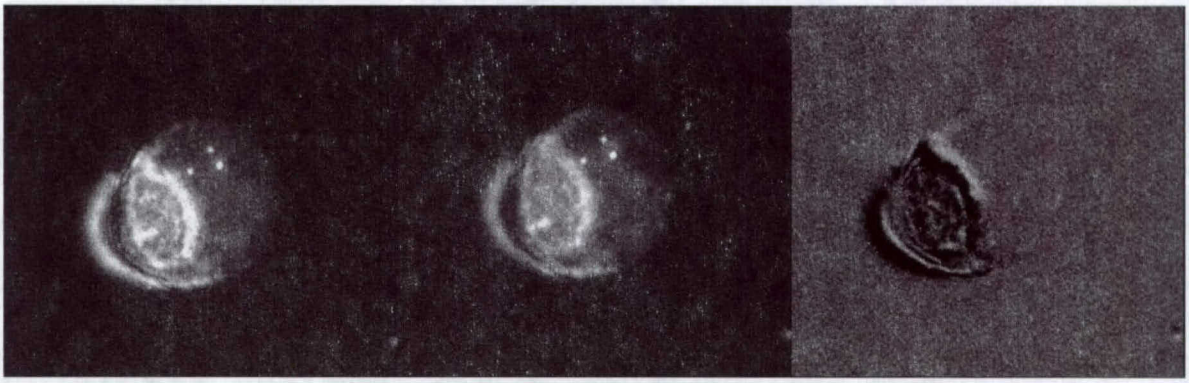

Figure 43. Roving moonlight from an out of focus 2 μm Brownian MOON rotating above a macrophage. (a) and (b) are images separated by 1 second. Three 300 nm Brownian MOONs in different orientations (brightnesses) are also visible inside the macrophage, although they did not rotate in this short time interval. An auotofluorescent background from the macrophage is also visible. (c) Shows the difference image, (a) minus image (b) resulting from the rotating Brownian MOON.

ii) Friction

Measurement of Friction/Rolling traction using MagMOONs

If the MagMOONs settle to a surface, they are observed to translate as they rotate around the center of pressure, rolling on the surface. For example, two ~4.5um MagMOONs in a solution on a glass slide were rotated simultaneously with a magnetic field and observed to roll an average of 0.35 +/-0.3 particle diameters each revolution; compared to a no slip condition, where the particle would roll π diameters per revolution, this corresponds to a traction efficiency of (11+/- 1)%. The rate of rolling depends on the particle size and shape, and surface interactions resulting in separation based on size and chemistry, if given sufficient distance. We observed the rolling traction depended on position and time (varying from 4% to 36%). Observing friction and slip is a novel method for the study of surface interactions on the micro and nano-scale as a function of rotation rate, surface properties, particle surface properties (on both metal capped and uncoated sides), shape of particle, and pressure normal to the surface. In an inhomogeneous medium, the surface interactions can occur in three dimensions, and direction of rolling could give insight into the local structure of the medium around the particle.

iii) Observation of Vorticity with Brownian MOONs

We have also observed Brownian MOONs rotating due to vorticity in fluid flow. A solution of 2 μm or 3.4 μm Brownian MOONs in a solution are observed to rotate and blink

when the fluid flows due to evaporation in a 100 μm demountable glass cell (Starna). They are also observed to rotate in flow due to wetting of a roughened microscope slide. In the later case, the flow is irregular, and the rotation rate depends strongly on particle position. A similar method of measuring viscosity is to use microspheres encapsulating flat reflective crystals, and measure the rate of flashing from reflection off the rotating crystal (US Pat 4385830). The use of MOONs allows a more continuous measurement of angle, and more uniform probes.

g) Summary:

During the grant period, we expanded our capabilities for MagMOONs fabrication, while developing new applications and techniques for the MagMOON platform. We made MagMOONs that sense pH, developed a general method to deposit magnetic half-shells onto nanospheres to make MagMOONs with uniform magnetic properties from nanospheres with a wide range of sizes and compositions. In addition, we improved our immunoassay techniques and developed new techniques of measuring local viscosity, and friction/rolling traction on a single MOON level. We also used 300 nm Brownian MOONs to observe biomechanical rotation of single MOONs inside living macrophages (figure 2). These tools have promising applications for disease detection and diagnosis, measuring material properties and mechanical forces on the nanoscale, and observing cell response to drug candidates and other stimuli.

Reference List

1. Xu, H., Yan, F., Monson, E.E., Kopelman, R.: Room-Temperature Preparation and Characterization of Poly (Ethylene Glycol)-Coated Silica Nanoparticles for Biomedical Applications. *Journal of Biomedical Materials Research Part a*. **66A**, 870-879, **2003**

2. Xu, H., Aylott, J.W., Kopelman, R., Miller, T.J., Philbert, M.A.: A Real-Time Ratiometric Method for the Determination of Molecular Oxygen Inside Living Cells Using Sol-Gel-Based Spherical Optical Nanosensors With Applications to Rat C6 Glioma. *Analytical Chemistry*. **73**, 4124-4133, **2001**

3. Park, E.J., Brasuel, M., Behrend, C., Philbert, M.A., Kopelman, R.: Ratiometric Optical PEBBLE Nanosensors for Real-Time Magnesium Ion Concentrations Inside Viable Cells. *Analytical Chemistry*. **75**, 3784-3791, **2003**

4. Helmlinger, G., Yuan, F., Dellian, M., Jain, R.K.: Interstitial Ph and Po(2) Gradients in Solid Tumors in Vivo: High-Resolution Measurements Reveal a Lack of Correlation. *Nature Medicine*. **3**, 177-182, **1997**

5. Ishiyama, K., Sendoh, M., Yamazaki, A., Arai, K.I.: Swimming Micro-Machine Driven by Magnetic Torque. *Sensors and Actuators a-Physical*. **91**, 141-144, **2001**

6. Born, M., Wolf, E.: *Principles of Optics--6th Ed, Chapter 13*. New York, NY, Cambridge University Press, **1980**.

7. Li, H.Y., Park, S.H., Reif, J.H., Labean, T.H., Yan, H.: Dna-Templated Self-Assembly of Protein and Nanoparticle Linear Arrays. *Journal of the American Chemical Society*. **126**, 418-419, **2004**

8. Daniel, M.C., Astruc, D.: Gold Nanoparticles: Assembly, Supramolecular Chemistry, Quantum-Size-Related Properties, and Applications Toward Biology, Catalysis, and Nanotechnology. *Chemical Reviews*. **104**, 293-346, **2004**

9. Lin, Y., Skaff, H., Emrick, T., Dinsmore, A.D., Russell, T.P.: Nanoparticle Assembly and Transport at Liquid-Liquid Interfaces. *Science*. **299**, 226-229, **2003**

10. Whitesides, G.M., Grzybowski, B.: Self-Assembly at All Scales. *Science*. **295**, 2418-2421, **2002**

11. Nicewarner-Pena, S.R., Freeman, R.G., Reiss, B.D., He, L., Pena, D.J., Walton, I.D., Cromer, R., Keating, C.D., Natan, M.J.: Submicrometer Metallic Barcodes. *Science*. **294**, 137-141, **2001**

12. Sanchez, C., Soler-Illia Gjda, Ribot, F., Lalot, T., Mayer, C.R., Cabuil, V.: Designed Hybrid Organic-Inorganic Nanocomposites From Functional Nanobuilding Blocks. *Chemistry of Materials*. **13**, 3061-3083, **2001**

13. Reculusa, S., Poncet-Legrand, C., Ravaine, S., Mingotaud, C., Duguet, E., Bourgeat-Lami, E.: Syntheses of Raspberrylike Silica/Polystyrene Materials. *Chemistry of Materials*. **14**, 2354-2359, **2002**

14. Fleming, M.S., Mandal, T.K., Walt, D.R.: Nanosphere-Microsphere Assembly: Methods for Core-Shell Materials Preparation. *Chemistry of Materials*. **13**, 2210-2216, **2001**

15. Kulbaba, K., Resendes, R., Cheng, A., Bartole, A., Safa-Sefat, A., Coombs, N., Stover, H.D.H., Greedan, J.E., Ozin, G.A., Manners, I.: Polyferrocenylsilane and Magnetic Ceramic Microspheres. *Advanced Materials*. **13** , 732-736, **2001**

16. Percy, M.J., Barthet, C., Lobb, J.C., Khan, M.A., Lascelles, S.F., Vamvakaki, M., Armes, S.P.: Synthesis and Characterization of Vinyl Polymer-Silica Colloidal Nanocomposites. *Langmuir*. **16**, 6913-+**2000**

17. Thurmond, K.B., Kowalewski, T., Wooley, K.L.: Shell Cross-Linked Knedels: a Synthetic Study of the Factors Affecting the Dimensions and Properties of Amphiphilic Core-Shell Nanospheres. *Journal of the American Chemical Society*. **119**, 6656-6665, **1997**

18. Grzybowski, B.A., Stone, H.A., Whitesides, G.M.: Dynamic Self-Assembly of Magnetized, Millimetre-Sized Objects Rotating at a Liquid-Air Interface. *Nature*. **405**, 1033-1036, **2000**

19. Martin, J.E., Venturini, E., Gulley, G.L., Williamson, J.: Using Triaxial Magnetic Fields to Create High Susceptibility Particle Composites. *Physical Review E*. **69**,**2004**

20. Salem, A.K., Chao, J., Leong, K.W., Searson, P.C.: Receptor-Mediated Self-Assembly of Multi-Component Magnetic Nanowires. *Advanced Materials*. **16**, 268-+**2004**

21. Sun, S.H., Anders, S., Hamann, H.F., Thiele, J.U., Baglin, J.E.E., Thomson, T., Fullerton, E.E., Murray, C.B., Terris, B.D.: Polymer Mediated Self-Assembly of Magnetic Nanoparticles. *Journal of the American Chemical Society*. **124**, 2884-2885, **2002**

22. Tanase, M., Bauer, L.A., Hultgren, A., Silevitch, D.M., Sun, L., Reich, D.H., Searson, P.C., Meyer, G.J.: Magnetic Alignment of Fluorescent Nanowires. *Nano Letters*. **1**, 155-158, **2001**

23. Klokkenburg, M., Vonk, C., Claesson, E.M., Meeldijk, J.D., Erne, B.H., Philipse, A.P.: Direct Imaging of Zero-Field Dipolar Structures in Colloidal Dispersions of Synthetic Magnetite. *Journal of the American Chemical Society*. **126**, 16706-16707, **2004**

24. Puntes, V.F., Krishnan, K.M., Alivisatos, A.P.: Colloidal Nanocrystal Shape and Size Control: the Case of Cobalt. *Science*. **291**, 2115-2117, **2001**

25. Love, J.C., Urbach, A.R., Prentiss, M.G., Whitesides, G.M.: Three-Dimensional Self-Assembly of Metallic Rods With Submicron Diameters Using Magnetic Interactions. *Journal of the American Chemical Society*. **125**, 12696-12697, **2003**

26. Urbach, A.R., Love, J.C., Prentiss, M.G., Whitesides, G.M.: Sub-100 Nm Confinement of Magnetic Nanoparticles Using Localized Magnetic Field Gradients. *Journal of the American Chemical Society*. **125**, 12704-12705, **2003**

27. Kneipp, K., Haka, A.S., Kneipp, H., Badizadegan, K., Yoshizawa, N., Boone, C., Shafer-Peltier, K.E., Motz, J.T., Dasari, R.R., Feld, M.S.: Surface-Enhanced Raman Spectroscopy in Single Living Cells Using Gold Nanoparticles. *Applied Spectroscopy*. **56**, 150-154, **2002**

28. Anker, J.N., Horvath, T.D., Kopelman, R.: Cooking with nanoparticles: A simple method of forming roll, pancake, and breaded polystyrene microparticles. , *European Cells and Materials*. **3**, 95**2002**

29. Anker, J.N., Behrend, C., Kopelman, R.: Aspherical Magnetically Modulated Optical Nanoprobes (Magmoons). *Journal of Applied Physics*. **93**, 6698-6700, **2003**

30. Behrend C.J. , Anker J.N., Kopelman R.: Brownian Modulated Optical Nanoprobes. *Applied Physics Letters*. **84**, 154-156, **2004**

31. Anker, J.N., Kopelman, R.: Magnetically Modulated Optical Nanoprobes. *Applied Physics Letters*. **82**, 1102-1104, **2003**

32. Takei, H., Shimizu, N.: Gradient Sensitive Microscopic Probes Prepared by Gold Evaporation and

Chemisorption on Latex Spheres. *Langmuir*. **13**, 1865-1868, **1997**

33. Cameron, L.A., Footer, M.J., Van Oudenaarden, A., Theriot, J.A.: Motility of Acta Protein-Coated Microspheres Driven by Actin Polymerization. *Proceedings of the National Academy of Sciences of the United States of America*. **96**, 4908-4913, **1999**

34. Link, J.R., Sailor, M.J.: Smart Dust: Self-Assembling, Self-Orienting Photonic Crystals of Porous Si. *Proceedings of the National Academy of Sciences of the United States of America*. **100**, 10607-10610, **2003**

35. Crowley, J.M., Sheridon, N.K., Romano, L.: Dipole Moments of Gyricon Balls. *Journal of Electrostatics*. **55**, 247-259, **2002**

36. Anker, J.N., Behrend, C.J., McNaughton, B.H., Roberts, T.G., Brasuel, M., Philbert, M.A., Kopelman, R.: Characterization and Applications of Modulated Optical Nanoprobes (MOONs). *2004 Proceedings of the Materials Research Society*.

37. Santhanam, V., Andres, R.P.: Microcontact Printing of Uniform Nanoparticle Arrays. *Nano Letters*. **4**, 41-44, **2004**

38. Mackintosh, F.C., Schmidt, C.F.: Microrheology. *Current Opinion in Colloid & Interface Science*. **4**, 300-307, **1999**

39. Nicolas, Y., Paques, M., Knaebel, A., Steyer, A., Munch, J.P., Blijdenstein, T.B.J., Van Aken, G.A.: Microrheology: Structural Evolution Under Static and Dynamic Conditions by Simultaneous Analysis of Confocal Microscopy and Diffusing Wave Spectroscopy. *Review of Scientific Instruments*. **74**, 3838-3844, **2003**

40. Breedveld, V., Pine, D.J.: Microrheology as a Tool for High-Throughput Screening. *Journal of Materials Science*. **38**, 4461-4470, **2003**

41. Van Vliet, K.J., Bao, G., Suresh, S.: The Biomechanics Toolbox: Experimental Approaches for Living Cells and Biomolecules. *Acta Materialia*. **51**, 5881-5905, **2003**

42. Zohar, O., Ikeda, M., Shinagawa, H., Inoue, H., Nakamura, H., Elbaum, D., Alkon, D.L., Yoshioka, T.: Thermal Imaging of Receptor-Activated Heat Production in Single Cells. *Biophysical Journal*. **74**, 82-89, **1998**

43. Monson, E., Brasuel, M., Philbert, M.A., Kopelman, R.: PEBBLE nanosensors for *in vitro* bioanalysis. In: Vo-Dinh, T., ed., *Biomedical Photonics Handbook*, CRC Press , **2003**,

44. Clark, H.A., Hoyer, M., Parus, S., Philbert, M.A., Kopelman, M.: Optochemical Nanosensors and Subcellular Applications in Living Cells. *Mikrochimica Acta*. **131**, 121-128, **1999**

45. Xu, H., Aylott, J.W., Kopelman, R.: Fluorescent Nano-Pebble Sensors Designed for Intracellular Glucose Imaging. *Analyst*. **127**, 1471-1477, **2002**

46. Aylott, J.W.: Optical Nanosensors - an Enabling Technology for Intracellular Measurements. *Analyst*. **128**, 309-312, **2003**

47. Brasuel, M., Kopelman, R., Miller, T.J., Tjalkens, R., Philbert, M.A.: Fluorescent Nanosensors for Intracellular Chemical Analysis: Decyl Methacrylate Liquid Polymer Matrix and Ion Exchange-Based Potassium Pebble Sensors With Real-Time Application to Viable Rat C6 Glioma Cells. *Analytical Chemistry*. **73**, 2221-2228, **2001**

48. Behrend, C.J., Anker, J.N., McNaughton, B.H., Brasuel, M., Philbert, M.A., Kopelman, R.: Metal

Capped Brownian Modulated Optical Nanoprobes (MOONs): From Aqueous to Biological Microenvironments . *Journal of Physical Chemistry*. **108**, 10408-10414, **2004**

49. Choi, J., Zhao, Y.H., Zhang, D.Y., Chien, S., Lo, Y.H.: Patterned Fluorescent Particles as Nanoprobes for the Investigation of Molecular Interactions. *Nano Letters*. **3**, 995-1000, **2003**

50. Buck, S.M., Xu, H., Brasuel, M., Philbert, M.A., Kopelman, R.: Nanoscale Probes Encapsulated by Biologically Localized Embedding (Pebbles) for Ion Sensing and Imaging in Live Cells. *Talanta*. **63**, 41-59, **2004**

51. Valberg, P.A., Feldman, H.A.: Magnetic Particle Motions Within Living Cells - Measurement of Cytoplasmic Viscosity and Motile Activity. *Biophysical Journal*. **52**, 551-561, **1987**

52. Janson, L.W., Ragsdale, K., Lubyphelps, K.: Mechanism and Size Cutoff Bar Steric Exclusion From Actin-Rich Cytoplasmic Domains. *Biophysical Journal*. **71**, 1228-1234, **1996**

53. Buck, S.M., Koo, Y.E.L., Park, E., Xu, H., Philbert, M.A., Brasuel, M.A., Kopelman, R.: Optochemical Nanosensor Pebbles: Photonic Explorers for Bioanalysis With Biologically Localized Embedding. *Current Opinion in Chemical Biology*. **8**, 540-546, **2004**

54. Carden, A., Rajachar, R.M., Morris, M.D., Kohn, D.H.: Ultrastructural Changes Accompanying the Mechanical Deformation of Bone Tissue: a Raman Imaging Study. *Calcified Tissue International*. **72**, 166-175, **2003**

55. Tauler, R., Smilde, A., Kowalski, B.: Selectivity, Local Rank, 3-Way Data-Analysis and Ambiguity in Multivariate Curve Resolution. *Journal of Chemometrics*. **9**, 31-58, **1995**

56. Shankar, P.N., Kumar, M.: Experimental-Determination of the Kinematic Viscosity of Glycerol Water Mixtures. *Proceedings of the Royal Society of London Series a- Mathematical Physical and Engineering Sciences*. **444**, 573-581, **1994**

57. Glogauer, M., Ferrier, J., Mcculloch, C.A.G.: Magnetic-Fields Applied to Collagen-Coated Ferric-Oxide Beads Induce Stretch-Activated Ca2+ Flux in Fibroblasts. *American Journal of Physiology-Cell Physiology*. **38**, C1093-C1104**1995**

Personnel Supported

Graduate students:
Jeffrey Anker,
Caleb Behrend,
Tom Horvath
Brandon McNaughton,
Gail Roberts.

Post Doctoral Fellows:
Dr. Murphy Brasuel.
Dr. Fei Yan
Dr. De Gao,
Dr. Hongmei Huang,
Dr. Katherine Tyner.

Professors
Professor Raoul Kopelman,
Professor Martin Philbert.

Publications

1. Behrend C. J., Anker J.N., Kopelman, R.: "Brownian modulated optical nanoprobes." *Applied Physics Letters*. **84**, 154-156, **2004.** [reprint enclosed]

This article was reviewed in Laser Focus World.

2. Anker J.N., Behrend C.J., McNaughton B.H., Roberts T.G., Brasuel M., Philbert M.A.: "Characterization and Applications of Modulated Optical Nanoprobes (MOONs)" *Mat. Res. Soc. Symp. Proc.* **790**, 4.4.1-12, **2004.** [Reprint Enclosed.]

3. Yan F., Xu H., Anker J.N., Kopelman R., Ross B., Rehemtulla A., Reddy R.: "Synthesis and Characterization of Silica-Embedded Iron Oxide Nanoparticlces for Magnetic Resonance Imaging." *Journal of Nanoscience and Nanotechnology:* **4**, 72-76, **2004.** [Reprint Enclosed.]

4. Behrend C.J., Anker J.N., McNaughton B.H., Roberts T.G., Brasuel M., Philbert M.A., Kopelman R.: "Metal-Capped Brownain and Magnetically Modulated Optical Nanoprobes (MOONs): Micromechanics in Chemical and Biological Microenvironments." *Journal of Physical Chemistry B:* **108**, 10408-10414, **2004.**
[Reprint Enclosed.]

5. Buck S.M., Xu H., Brasuel M., Philbert M.A., Kopelman R.: "Nanoscale probes encapsulated by biologically localized embedding (PEBBLEs) for ion sensing and imaging in live cells." *Talanta*: **63** (1), 41-59. (2004)
[Reprint Enclosed.]

6. Anker J.N., Behrend C.J., McNaughton B.H., Roberts T.G., Kopelman R.: "magnetically modulated optical nanoprobes (MagMOONs) and systems." *Journal of Magnetism and Magnetic Materials:* **293**, 655-662, (2005).
[Reprint Enclosed.]

7. Behrend C.J., Anker J.N., McNaughton B.H., Kopelman R.: "Microrheology with Modulated Optical Nanoprobes (MOONs)." *Journal of Magnetism and Magnetic Materials:* **293**, 663-670, (2005).
[Reprint Enclosed.]

8. McNaughton B.H., Anker J.N., Kopelman R.: "Magnetic microdrill as a modulated fluorescent pH sensor." *Journal of Magnetism and Magnetic Materials:* **293**, 696-701, (2005).
[Reprint Enclosed.]

9. Roberts T.G., Anker J.N., Kopelman R.: "Magnetically Modulated Optical Nanoprobes (MagMOONS) for Detection and Quantification of Biologically Important Ions against the Natural Background Fluorescence of Intracellular Environments." *Journal of Magnetism and Magnetic Materials:* **293**, 715-724, (2005).
[Reprint Enclosed.]

10. Anker J.N.: "Modulated Optical Nanoprobes (MOONs) in the NanoKitchen." University of Michigan, Ann Arbor, MI. 2005.

11. McNaughton B.H., Stoica V., Anker J.N., Clarke R., Kopelman R.: "Fabrication of Uniform Magnetic Nanoparticles and Microparticles with Applications as Magnetically Modulated Optical Nanoprobes" *Applied Physics Letters.* (Submitted). [Manuscript Enclosed.]

12. Huang H., Anker J.N., Wang K., Kopelman R.: "Magnetically assisted self-assembly into strawberry-like microparticles." *In Preparation.*

Interactions/Transactions

MagneSensors:

We collaborated with Dr. DiIorio, at.MagneSensors Inc. We mailed him samples of 100-200nm silica magnetic nanoparticles containing iron oxide produced by Dr. Fei Yan. The particles were originally for use as MRI contrast agents for an NCI contract.

Dr. Raoul Kopelman agreed to serve as a consultant to MagneSensors Inc. (Dr. Mark DiIorio, P.I.)

Nanoplex

Nanoplex produces nanorods with striped barcode patterns for highly multiplexed solution phase immunoassays. We recently obtained specially made nanorods containing magnetic material for modulation and streptavidin for chemical binding. We may experiment with these for aspherical MagMOON assays.

Molecular Beam Epitaxy (MBE)

We are collaborating with Professor Roy Clarke at the University of Michigan produce MagMOONs using MBE deposition of magnetic materials.

Conferences:

BiomagnetICs

The following members of our lab group attended the Biomagnetics Kickoff Conference:

Jeffrey Anker,
Gail Roberts,
Brandon McNaughton,
Caleb Behnrend,
Professor Raoul Kopelman

University of Michigan Applied Physics Symposium (Ann Arbor, MI 2003)

Jeffery Anker
Brandon McNaughton

Syposium on Nanotechnology in Honor of Dr. Raoul Kopelman's 70th Birthday (Ann Arbor, November 2003)

Dr. Raoul Kopelman,
Dr. Martin Philbert,
Dr. Fei Yan
Dr. Murphy Brasuel
Jeffrey Anker,
Caleb Behrend,
Brandon McNaughton,
Gail Roberts.

PITTCON Conference (Chicago, March 2004).

The following DARPA-supported members of our lab group attended and presented:

Jeffrey Anker,
Brandon McNaughton,
Dr. Raoul Kopelman.

Magnetic Carriers Conference (Lyon, May 2004).
The following members of our lab group attended the Conference on Scientific and Clinical Applications of Magnetic Microspheres:

Jeffrey Anker,
Brandon McNaughton,
Caleb Behrend,
Dr. Raoul Kopelman

BiomagnetICs PI Review (Potomac Maryland, September 2004)
The following members of our lab group attended the Biomagnetics Conference in Maryland:

Jeffrey Anker,
Brandon McNaughton,
Caleb Behnrend,
Professor Raoul Kopelman

New discoveries, inventions or patent disclosures.
Brownian MagMOONs.

On April 18th 2003, just prior to start of the DARPA grant. Jeffrey Anker, Dr. Eric Monson, Dr. Raoul Kopelman (P.I), and Dr. Martin Philbert (P.I.) filed a patent application for "Modulated Chemical Sensors."

On June 29th, 2005, Dr. Jeffrey Anker, Caleb Behrend, Brandon McNaughton, and Dr. Raoul Kopelman (P.I.) Filed a continuation-in-part patent application, titled "Modulated Physical and Chemical Sensors."

Honors/Awards:

Jeffrey Anker

$700 Rackham travel grant.
Rackham Predoctoral Fellowship (Stipend and tuition).
2002 National Inventor's Hall of Fame Collegiate Inventor's Competition $33,000 Grand Prize winner. , See ww.invent.org/collegiate/2002winners/winner1.html
Ph.D. University of Michigan February 2005.

Caleb Behrend,

$700 Rackham travel grant.
Molecular Biophysics Training Grant (Stipend and tuition).

Brandon McNaughton,

$700 Rackham travel grant,
150 Euros grant from the Magnetic Carriers Conference based on abstract merit.

Jeffrey Anker, Caleb Behrend, Brandon McNaughton, Howard Lin, Nathan Stone.
Pryor Hale Business Competition finalists.

Dr. Martin Philbert
Associate Dean of the School of Public Health, University of Michigan.

Dr. Raoul Kopelman,
Syposium on Nanotechnology in Honor of Dr. Raoul Kopelman's 70th Birthday, (Ann Arbor, November 2003).
ACS Edward Morley Award and Medal, 1997.